OFDM WITH INDEX MODULATION FOR NARROWBAND IOT AND MMTC

A THESIS SUBMITTED TO

THE GRADUATE SCHOOL OF

ENGINEERING AND NATURAL SCIENCES

OF ISTANBUL MEDIPOL UNIVERSITY

IN PARTIAL FULFILLMENT OF THE REQUIREMENTS FOR

THE DEGREE OF

MASTER OF SCIENCE

IN

ELECTRICAL-ELECTRONICS ENGINEERING AND CYBER SYSTEMS

By
Armed Tusha
July, 2018

This thesis work is dedicated to my family, who has been a constant source of support and encouragement during the challenges of graduate school and life. I am truly thankful for having you in my life.

ABSTRACT

OFDM WITH INDEX MODULATION FOR NARROWBAND IOT AND MMTC

Armed Tusha

M.S. in Electrical-Electronics Engineering and Cyber Systems

Advisor: Prof. Dr. Hüseyin Arslan

July, 2018

The crucial aim for 5G narrowband Internet of Things (NB-IoT) is to support massive Machine-Type Communications (mMTC) with wide coverage area, low power consumption, low hardware complexity and low data rate. Direct conversion receiver (DCR) has a simple structure to fulfill NB-IoT requirements. However, a significant degradation has been observed on the performance of orthogonal frequency division multiplexing (OFDM) systems with DCR due to in-phase and quadrature-phase imbalance (IQI) at RF front-end. Estimation and mitigation of IQI in OFDM systems require iterative receiver at the expense of high complexity and power consumption. In this study, OFDM with index modulation (OFDM-IM) is proposed as a promising candidate in order to meet demands of NB-IoT use cases. OFDM-IM based systems carry data information not only by modulated subcarriers but also by indices of fractionally used subcarriers. A non-iterative and efficient receiver that exploits inactive subcarriers is introduced to mitigate the effect of IQI for NB-IoT with OFDM-IM. Cyclic Redundancy Check (CRC) algorithm is used to investigate accuracy of the receiver under IQI. Theoretical analysis and computer-based simulations show that proposed non-iterative receiver for OFDM-IM in NB-IoT under IQI works very well in various scenarios. Moreover, our findings show that OFDM-IM under IQI provides a higher signal-to-interference ratio (SIR) in comparison to classical OFDM. In mMTC systems, lack of coordination between the machine users and the BS in time destroys orthogonality between the subcarriers, and causes intercarrier interference (ICI). Unlike classical OFDM, fractional subcarrier activation leads to less ICI in OFDM-IM technology. Furthermore, a novel subcarrier mapping scheme (SMS) named as Inner Subcarrier Activation is proposed to further alleviate adjacent user interference in asynchronous OFDM-IM based systems.

Keywords: IQI, NB-IoT, non-iterative estimation and mitigation, OFDM with

index modulation (OFDM-IM), asynchronous transmission, massive Machine-Type Communication (mMTC).

ÖZET

DAR BANT NESNELERİN İNTERNETİ VE KİTLESEL MAKİNE TİPİ HABERLEŞME İÇİN İNDEKS MODÜLASYONLU OFDM

Armed Tusha

Elektrik-Elektronik Mühendisliği ve Siber Sistemler, Yüksek Lisans

Tez Danışmanı: Prof. Dr. Hüseyin Arslan

Temmuz, 2018

5G Dar bant nesnelerin interneti için kritik amaç; geniş kapsama alanı, düşük güç tüketimi, düşük donanım karmaşıklığı ve düşük data oranı sağlayan toplu makine tipi haberleşme sistemlerini desteklemektir. Dar bant - nesnelerin internetin gereksinimleri karşılamak için, doğrudan dönüşüm sağlayan alıcı sistemleri basit bir yapıya sahiptir. Fakat, dikgen frekans bölmeli çoğullama sistemlerinin performansında önemli ölçüde doğrudan dönüşüm sebebi ile bozulma gözlemlenmektedir. Bu bozunum I ve Q dalları arasındaki genlik ve faz farkından kaynaklanmaktadır. Dikgen frekans bölmeli çoğullama sistemlerinde I ve Q dalları arasındaki dengesizliğin tahmini ve telafi edilmesi tekrarlamalı alıcı gerektirmektedir. Tekrarlamalı alıcı, güç tüketimine ve yüksek karmaşıklığa sebep olmaktadır. Bu çalışmada, indis modülasyonlu dikgen frekans bölmeli çoğullama dar bant nesnelerin interneti için önerilmektedir. İndis modülasyonlu dikgen frekans bölmeli çoğullama sadece modülasyonlu alt taşıyıcı ile değil kullanılan alt taşıyıcının indisi ile veri iletimine izin vermektedir. Aktif olmayan alt taşıyıcıların kullanımı ile tekrarlamalı olmayan ve verimli alıcı yapısı I ve Q dalları arasındaki dengesizliği kaldırmak için tanıtıldı. Önerilen alıcı yapısının doğruluğu, çevrimsel artıklık kontrol algoritması ile araştırıldı. Teorik analizler ve bilgisayar tabanlı simülasyonlar indis modülasyonlu dikgen frekans bölmeli çoğullama kullanılarak önerilen alıcı yapısı ile çeşitli senaryolarda I ve Q dalları arasındaki dengesizliğin tahmini ve telafisinin gerçekleştirildiğini göstermektedir. Ek olarak, elde edilen sonuçlara göre indis modülasyonlu dikgen frekans bölmeli çoğullama günümüz teknolojisi dikgen frekans bölmeli çoğullamaya göre yüksek sinyal-girişim oranı sağlamaktadır.

Makine tipi haberleşme sistemlerinde, baz istasyonu ve makina kullanıcılar

arasında koordinasyon olmaması dikgen frekans bölmeli çoğullama sistemlerinde alt taşıyıcılar arasındaki dikgenliği bozmakta ve alt taşıyıcılar arası girişime sebep olmaktadır. İndis modülasyonlu dikgen frekans bölmeli çoğullama ile kısmi alt taşıyıcı kullanımı alt taşıyıcılar arasında daha az girişime sebep olmaktadır. Asenkron indis modülasyonlu dikgen frekans bölmeli çoğullama tabanlı sistemlerde komşu kullanıcılardan gelen girişimi önlemek için yeni alt taşıyıcı kullanım şeması tanıtıldı.

Anahtar sözcükler: IQI, dar bant nesnelerin interneti, tekrarlayıcı olmayan tahmin ve azaltma, indeks modülasyonlu OFDM (OFDM-IM), asenkron iletim, kitlesel makine tipi iletişim (mMTC).

Acknowledgement

Foremost, I want to thank our God Almighty, who continues to make the impossible possible, for giving me the strength, knowledge, ability and opportunity to undertake this research study and to persevere and complete it satisfactorily.

I would like to express my sincere gratitude to my advisor Prof. Dr. Hüseyin Arslan for the continuous support of my master study and related research, for his motivation, and immense knowledge. His guidance helped me in all the time of research and writing of this thesis. I wish to thank individually Assoc. Prof. Dr. Ertuğrul Başar and Assoc. Prof. Dr. Tunçer Baykaş for agreeing to serve in my committee; and for their valuable time, feedback, and recommendations. Also, I would like to thank Assoc. Prof. Dr. M. Kemal Özdemir for his precious help and time during my undergraduate, and master studies. Without his unconditional support and profound wisdom, I would not be here today. I am grateful to my colleagues at CoSiNC research group with whom I have had the pleasure to work during this and other related projects. I would especially like to thank my research mate Mrs. Seda Doğan for her sincere support and limitless contribution throughout the conduction of this research work.

Nobody has been more important to me in the pursuit of this work than the members of my family to whom this work is dedicated. I would like to thank my parents and my two lovely sisters, whose love and guidance are with me in whatever I pursue.

Contents

List of Figures

List of Tables

Chapter 1

Introduction

In the last decade, evolution of 5G networks is becoming a major driver for growth of Internet of Things (IoT) applications. Therefore, preliminary interest of communication researchers and engineers has been to develop communication systems for 5G and beyond technology. The aim is to satisfy various demands set by the current and future user based applications. Most important usage scenarios for next generation wireless systems are enhanced Mobile Broadband (eMBB), massive Machine-Type Communications (mMTC), and Ultra-Reliable and Low-Latency Communication (URLLC).

Recently, the proliferation of index modulation (IM)[1] has introduced new research perspectives for 5G wireless systems. IM is applied to orthogonal frequency division multiplexing (OFDM) by activating subcarriers partially, and it is called as OFDM with index modulation (OFDM-IM). In this dissertation, performance of IM in OFDM based system is analysed regarding different user applications for wireless systems.

In first chapter, performance of in-phase and quadrature-phase imbalance (IQI) with OFDM-IM for Narrowband Internet of Things (NB-IoT) is investigated in detail, and a blind non-iterative receiver is proposed to mitigate IQI [2]. Moreover,

---

[1]Concept of index modulation is explained in chapter 1

[2]IQI model and blind non-iterative receiver are explained in chapter 1

our findings show that OFDM-IM under IQI provides higher signal-to-interference ratio (SIR) in comparison to classical OFDM.

In the second chapter, it is investigated asynchronous transmission with OFDM-IM for mMTC. A novel subcarrier mapping scheme (SMS) named as Inner Subcarrier Activation [3] is proposed to further alleviate adjacent user interference in asynchronous OFDM-IM-based systems.

---

[3]SMS are explained in chapter 2

Chapter 2

IQI Mitigation for Narrowband IoT Systems with OFDM-IM

2.1 Introduction

Narrowband Internet of Things (NB-IoT) provides Low Power Wide Area (LPWA) coverage via massive devices for next-generation use cases and applications [1, 21, 47]. In order to make massive connections possible over devices, NB-IoT should meet key performance requirements of IoT. The key requirements consist of user equipment (UE) with low complexity, low power consumption, long battery life and deployment flexibility [1, 4, 47]. For instance, smart metering and smart agriculture reduce cost and improve service quality by remotely accessing the devices, while smart parking reduces traffic and car accidents by connected vehicles. Some use cases for NB-IoT technology are illustrated in Fig. 2.1.

Conception of index modulation (IM) has provided novel and different perspectives to evaluate 5G and beyond communication systems [8]. Firstly, IM has been introduced as a spatial modulation (SM) technique for multi-input multi-output (MIMO) systems by transmitting additional information bits through antenna indices [32]. IM is then applied to orthogonal frequency division multiplexing
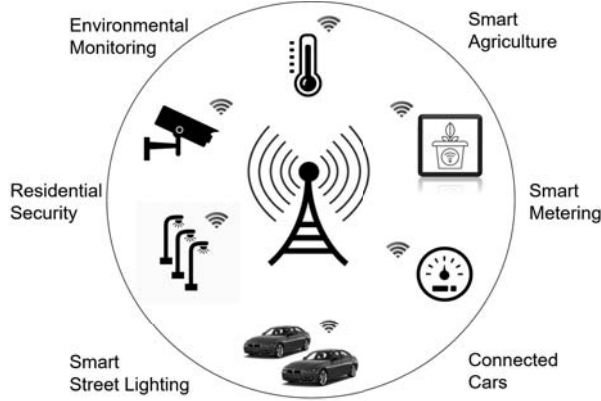
Figure 2.1: Use cases for NB-IoT .

(OFDM) by activating subcarriers partially, and it is called as OFDM with index modulation (OFDM-IM) [7]. In OFDM-IM, data information is carried not only by active subcarriers but also by their indices. Combination of conventional M-ary modulation with IM in OFDM-IM provides flexible and adaptable structure to exploit them properly regarding next-generation use cases requirements. Fractional activation of subcarriers in OFDM-IM leads to a significant improvement on error performance under frequency selective channel, Doppler impairment and inter-carrier interference (ICI) compared with conventional OFDM [7, 15, 28, 36]. Hence, it is proposed for vehicle to X (V2X) and uncoordinated networks such as massive machine-type communications (mMTC) [15, 18]. Since not all the subcarriers are activated and additional bits are carried by subcarrier indices, OFDM-IM provides power efficiency and diversity gain, too. Moreover, it allows increase on spectral efficiency for low order modulations in comparison to OFDM.

In this paper, OFDM-IM is considered as a promising candidate for NB- IoT due to motivations listed as follow.

- OFDM-IM is suitable for massive connections due to its flexible structure. Number of active subcarriers and type of M-ary modulation can be changed considering requirements of NB-IoT use case.

- OFDM-IM gives a chance to control power consumption by number of used subcarriers for data transmission.

4

- Limited available spectrum in NB-IoT systems results in reduced subcarrier spacing, which causes more sensitivity against ICI. Fortunately, partial subcarrier usage on OFDM-IM leads to less ICI in comparison to OFDM.

- NB-IoT is designed for low data rate up to 100 kbps [1]. Superiority of OFDM-IM against OFDM is obvious for low order modulation types. OFDM-IM provides both power efficiency and spectral efficiency for low order modulations such as binary phase shift keying (BPSK).

In order to offer low hardware complexity, direct conversion receiver (DCR) has been proposed for NB-IoT devices [13,25]. Since DCR neither uses image rejection filters nor intermediate frequency (IF), it allows low complex receiver and low power consumption [2]. Also, it provides easier integration with massive devices in comparison to super-heterodyne receiver (SHR) due to its simple structure. However, direct conversion of a signal from baseband to radio frequency (RF) or vice versa at DCR causes more distortion at the signal. This is due to in-phase and quadrature imbalance (IQI) between modulator/demodulator branches [20, 39]. A simple receiver model with IQI is illustrated in Fig. 2.2. IQI corresponds to mismatches on the amplitude (ϵ) and phase ($\Delta\phi$) response of the local oscillators (LO) on I and Q branches. Ideally, both branches should consist of carriers with exactly the same signal level ($\epsilon = 0$) and $\pi/2$ phase difference ($\Delta\phi = 0$). Otherwise, IQI causes both in-band self degradation (IBSD) and in-band mirror interference (IBMI) in classical OFDM systems. In current technology OFDM, blind and data-aided iterative solutions are studied to suppress IQI impact [6, 27, 30, 35, 43, 44]. High number of iterations in blind techniques leads to high complexity, while use of training symbols in data-aided techniques causes loss of spectral efficiency. Hence, they are not suitable for NB-IoT applications.

To the best of author's knowledge, the impact of IQI for OFDM-IM-based systems has not been studied and characterized. In this work, frequency independent IQI is considered since IQI is independent from the frequency for narrowband communication systems [26]. This work proposes a non-iterative blind compensator to mitigate IQI by using inactive subcarriers in OFDM-IM data transmission. Compensation with OFDM-IM not only reduces low complexity

5
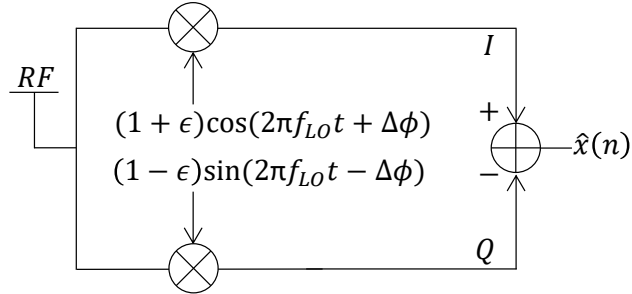
Figure 2.2: A simple direct-conversion receiver model with IQ imbalance.

but also provides less power consumption compared with iterative compensators, which are used in classical OFDM. Inactive subcarriers are used to localize IBSD and IBMI. In this way, localized IBSD and IBMI is used to estimate and compensate IQI impact. The main contributions of this paper are prioritized as follow:

- OFDM-IM is proposed for NB-IoT due to the aforementioned motivations.

- Use of DCR for NB-IoT systems causes a high IQI impact. To estimate and compensate this effect, a non-iterative receiver with OFDM-IM is proposed by exploiting inactive subcarriers during data transmission.

- Theoretical signal-to-interference-noise ratio (SINR) and average bit error probability (ABEP) analysis are performed for OFDM-IM under IQI.

The remainder of this work is organized as follows. Section 2 introduces OFDM-IM system model and IQI model. Section 3 presents proposed IQI compensator by OFDM-IM. Section 4 covers theoretical analysis for OFDM-IM considering IQI impact. Section 5 provides computer based simulation results and theoretical results. Finally, some concluding remarks are provided for NB-IoT with OFDM-IM in Section 6.

2.2 System Model

In this section, firstly OFDM-IM system model is revised regarding a receiver with ideal RF conversion ($\epsilon = 0, \Delta\phi = 0$). Later, imperfect RF conversion ($\epsilon \neq 0, \Delta\phi \neq 0$) is considered for OFDM-IM.

2.2.1 OFDM-IM System Model

In this work, it is considered a classical OFDM-IM block with N subcarriers, which are equally split into g subblocks. Block diagram of OFDM-IM transmitter is shown in Fig. 2.3. Each subblock contains $b = \frac{N}{g}$ subcarriers, where a out of b are selected to carry data information. Number of information bits conveyed by indices of active subcarriers per subblock is $p_1 = \lfloor log_2 C(b, a) \rfloor$, where $C(b, a)$ and $\lfloor . \rfloor$ denote binomial coefficient and floor function, respectively. Selected subcarrier indices for l-th subblock can be expressed as

$$\xi_l = [i_l(1), \ldots, i_l(a)]_{1 \times a} \tag{2.1}$$

where $i_l(v) \in [1, 2, \ldots, b]$. $p_2 = a(log_2 M)$ bits of information are mapped to M-ary data symbols $s_v = [s_1, \ldots, s_a]$. Transmitted symbols by selected subcarrier indices for l-th subblock is denoted as

Note that if $a = b$, the system turns into a conventional OFDM system. Later, "Block Generator" entity through composition of all g subblocks generates the OFDM-IM block, which is expressed as follow

$$X = [X_1(1), \ldots, X_g(b)]_{1 \times N}. \tag{2.2}$$

Total number of data bits assigned to one OFDM-IM block equals

$$m = gp = g(p_1 + p_2), \tag{2.3}$$
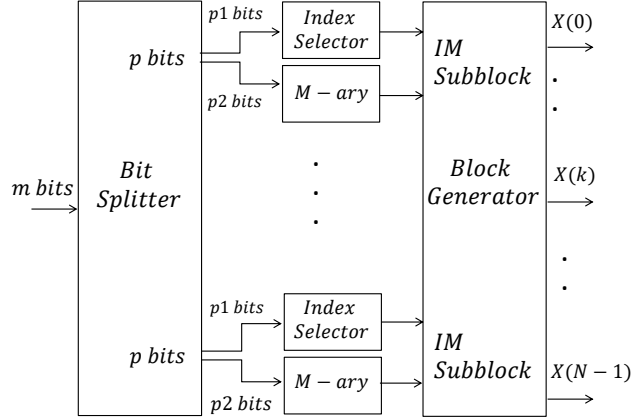
Figure 2.3: Block diagram for OFDM-IM transmitter and inverse process is performed for OFDM-IM receiver.

where $p = p_1 + p_2$ is the number of bits per OFDM-IM subblock.

Frequency domain signal X is transformed to time domain samples by Inverse Fast Fourier Transform (IFFT) after it passes through serial to parallel converter. The time domain samples of OFDM-IM symbol can be obtained as

$$x(n) = \sum_{k=0}^{N-1} X(k) e^{\frac{j2\pi nk}{N}}, \quad 0 \le n \le N-1. \tag{2.4}$$

A cycle prefix (CP) is generated by coping last samples of the time domain signal and appended to the beginning. CP size has to exceed maximum excess delay of the channel to prevent inter-symbol interference, which is caused by time dispersion of the channel [5]. After $x(n)$ leaves the transmitter, it undergoes through an independent and identically distributed (i.i.d.) multipath Rayleigh fading channel $h(n) = \sum_{l=0}^{L-1} h(l)\delta(n-l)$ as follow

$$y(n) = \sum_{l=0}^{L-1} h(l)x(n-l) + w(n), \tag{2.5}$$

where L is the number of channel taps, and path gains $h(l)$ are Gaussian random variables with $\mathcal{CN}(0, \frac{1}{L})$. $w(n)$ denotes additive white Gaussian noise (AWGN) with zero mean and variance σ_o^2.

At the receiver, CP is removed and then Fourier Transform (FFT) process is applied to the time domain signal to obtain frequency domain signal, which is

expressed as

$$Y(k) = \sum_{k=0}^{N-1} y(n)e^{\frac{-j2\pi nk}{N}}, \quad 0 \le n \le N-1. \tag{2.6}$$

The frequency domain signal for the k-th subcarrier $Y(k)$ is

$$Y(k) = \underbrace{X(k)}_{\text{desired signal}} H(k) + W(k), \tag{2.7}$$

where $H(k)$ is channel frequency response (CFR) $\sim \mathcal{CN}(0,1)$, and $W(k)$ represents frequency response of AWGN $\sim \mathcal{CN}(0, N_0)$.

In this work, active subcarrier indices ξ_l for l-th OFDM-IM subblock are detected by using log-likelihood ratio (LLR) receiver [49]. The receiver calculates LLR values $\lambda(k)$ for all subcarriers within the l-th subblock as

$$\lambda(k) = log\frac{a}{b-a} + \frac{|Y(k)^2|}{N_0} + log\frac{1}{M}\sum_{i=1}^{M}\frac{|Y(k) - H(k)s_i|}{N_0}. \tag{2.8}$$

For each subblock, a number of subcarriers with maximum λ values represent the active subcarrier indices. Then, the indices are mapped to bits to get p_1 bit stream [7]. Whilst, p_2 bit stream is obtained after demodulation of M-ary symbols, carried by the active subcarriers.

2.2.2 IQI Model

In a system, RF signal at the receiver $z(n)$ is converted to baseband signal $\hat{z}(n)$ via DCR. In this work, it is assumed that perfect low-pass filter (LPF) and analog-to-digital converter (ADC). In general, any imperfection on gain ($\epsilon \neq 0$) and phase ($\Delta\phi \neq 0$) between sine and cosine waveforms destroys their orthogonality, as illustrated in Fig. 2.2. The imbalance components between I and Q branches are modeled as [43]

$$\alpha = cos(\Delta\phi) + j\epsilon sin(\Delta\phi), \tag{2.9}$$

$$\beta = \epsilon cos(\Delta\phi) - j sin(\Delta\phi). \tag{2.10}$$

The time domain baseband signal with IQI $\hat{z}(n)$ can be represented as

$$\hat{z}(n) = \alpha z(n) + \beta z^*(n), \tag{2.11}$$

where $(.)^*$ denotes the complex conjugate. Since FFT of complex conjugate of the time domain signal $z^*(n)$ corresponds to complex conjugate of mirror subcarrier $Z^*(-k)$, frequency domain samples of $\hat{z}(n)$ are expressed as

$$\hat{Z}(k) = \alpha Z(k) + \beta Z^*(-k), \tag{2.12}$$

where $-k$ represents mirror subcarrier of k-th subcarrier and vice versa. As an example, in Fig. 2.4, dark blue subcarrier is mirror for blue subcarrier, while blue subcarrier is mirror for dark blue subcarrier. According to (2.12), α represents the degradation on subcarrier k, which is named as IBSD. β represents the interference on k-th subcarrier coming from its mirror $(-k)$-th subcarrier, which is named as IBMI. If I and Q branches perfectly match, $\alpha = 1$ and $\beta = 0$. So, there is no degradation on a subcarrier, and also zero interference comes from its imaginary subcarrier.

By substituting $Y(k)$ from (2.7) into $Z(k)$ of (2.12), frequency domain signal with IQI $\hat{Y}(k)$ is expressed as

$$\hat{Y}(k) = \alpha \underbrace{X(k)}_{\text{desired signal}} H(k) + \underbrace{\beta X^*(-k)H^*(-k)}_{\text{interference}} + \underbrace{W'(k)}_{\text{amplified noise}}, \tag{2.13}$$

where $W'(k) = \alpha W(k) + \beta W^*(-k)$ denotes the amplification of the noise due to IQI. $W'(k) \sim \mathcal{N}(0, N_0')$ has variance as

$$N_0' = (|\alpha|^2 + |\beta|^2)N_0 = (1 + \epsilon^2)N_0, \tag{2.14}$$

where the amplification of noise happens only due to gain imbalance ($\epsilon \neq 0$). Since the amplified noise $\epsilon^2 N_0$ is very small can be avoided.

2.3 IQI Mitigation with OFDM-IM

In this study, a non-iterative IQI compensator for NB-IoT systems is proposed by OFDM-IM to enhance system performance, reduce complexity and power

(a) OFDM
(b) OFDM-IM
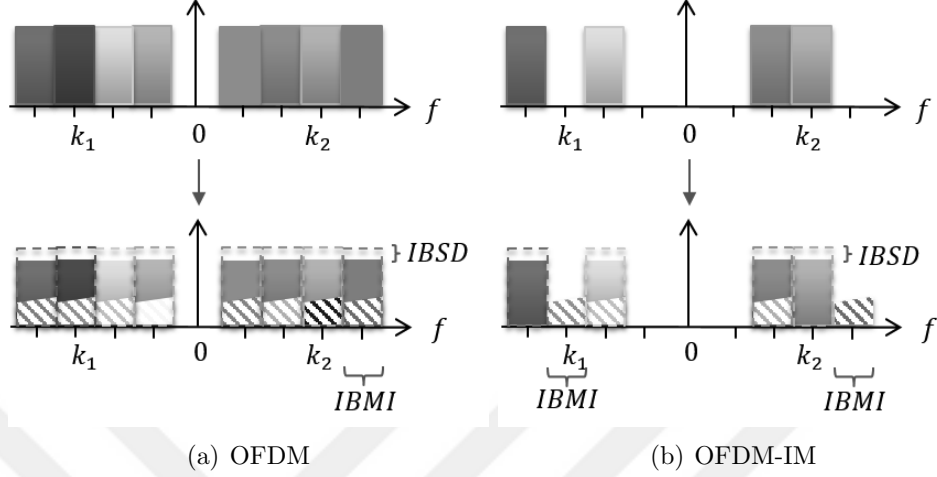
Figure 2.4: IQI impact for OFDM and OFDM-IM.

consumption.

A visualization of (2.13) is illustrated in Fig. 2.4 for OFDM and OFDM-IM. In Fig. 2.4a, IQI impact is shown for OFDM where each subcarrier suffers from both IBSD and IBMI. Due to partial activation of subcarriers in OFDM-IM, not all the subcarriers are effected from both IBSD and IBMI, as shown in Fig. 2.4b. Moreover, IBMI does not occur on the subcarriers with null mirror, and there is no IBSD on null subcarriers. In Fig. 2.4b, only IBSD is present in subcarrier k_2 since there is zero interference coming from its mirror subcarrier k_1. Hence, equivalent baseband signal for active $X(k) \neq 0$ and inactive $X(-k) = 0$ is expressed as

$$D(k) = \alpha X(k)H(k) + W'(k). \tag{2.15}$$

Similarly, only the IBMI which is coming from mirror subcarrier k_2 is present in subcarrier k_1. In this scenario, equivalent baseband signal for inactive $X(k) = 0$ and active $X(-k) \neq 0$ is expressed as

$$I(k) = \beta X^*(-k)H^*(-k)) + W'(k). \tag{2.16}$$

Estimation of IQI parameters α and β is more complex for OFDM due to accumulation of IBSD and IBMI within a subcarrier in comparison to OFDM-IM. Therefore, an iterative estimation is required to get IQI parameters. On the

other hand, there is no need to make a joined estimation for IQI components in OFDM-IM. Since $D(k)$ and $I(k)$ are linear functions of α and β regarding to (2.15) and (2.16), respectively. Therefore, α parameter is easily extracted from IBSD (2.15), and β is calculated from IBMI (2.16). In this way, α and β estimation are modeled as follow.

For active $X(k) \neq 0$ and inactive $X(-k) = 0$

$$\alpha = \frac{\hat{Y}(k)}{X(k)H(k)} + W'(k), \tag{2.17}$$

while for inactive $X(k) = 0$ and active $X(-k) \neq 0$

$$\beta = \frac{\hat{Y}(k)}{X^*(-k)H^*(-k)} + W'(k). \tag{2.18}$$

Regarding (2.17) and (2.18), subcarrier index status (active/inactive) and $X(k)$ are required to estimate the imbalance parameters α and β. To know subcarrier index status, LLR values $\lambda(k)$ are calculated from $\hat{Y}(k)$ for each sub-block at the receiver, as in (2.8). According to the obtained subcarrier index status, $X(k)$ is assumed as known by making a hard decision on $\hat{Y}(k)$, and is represented as $\hat{X}(k)$ [43]. Estimation of α and β components is performed by using both $\lambda(k)$ and $\hat{X}(k)$ values in one OFDM-IM block, regarding (2.17) and (2.18), respectively. To calculate ultimate α and β, all α and β values are averaged out over an OFDM-IM block. However, averaging the estimation of IQI components over more than one OFDM-IM block is needed for both high subcarrier activation ratio $\frac{a}{b}$ and IQI level. For these cases, required number of OFDM-IM blocks (N_B) is provided in Section V. The same IQI parameters, ultimate α and β, are applied to correct IQI at each block by considering (2.13) as

$$X'(k) = \frac{\hat{Y}(k) - \beta \hat{X}^*(-k)H^*(-k)}{\alpha H(k)}. \tag{2.19}$$

Later, corrected data symbols $X'(k)$ is mapped to $\hat{p}_1$ and $\hat{p}_2$ bit streams per subblock by considering the inverse process of block diagram in Fig. 2.3.

The main challenges for estimation of IQI components on narrowband OFDM-IM systems are active subcarrier indices detection and channel estimation. Increase on the number of active subcarriers degrades the accuracy of the proposed estimation technique. If all the subcarriers are utilized ($a = b$), OFDM-IM becomes a classical OFDM. Moreover, Cyclic Redundancy Check (CRC) algorithm is used to assess the robustness of the proposed compensator for various subcarrier activation ratio. A CRC-bit stream is appended at the end of the data bit stream per each OFDM-IM block. CRC is checked on data bits of $\hat{X}(k)$. Later, α and β components are estimated only for an OFDM-IM block with correct CRC. Necessity of CRC usage regarding activation ratio and IQI level is discussed in Section V. To assess the robustness of the proposed compensator against imperfect channel state information (CSI), intentional error Δh is added to the ideal channel $h(n)$. A complex AWGN $\sim \mathcal{N}(0, e10^{\frac{-\gamma_{idB}}{10}})$ is used to generate Δh, where e denotes the error amount of perfect CSI, and γ_{idB} represents signal-to-noise ratio (SNR) γ_i in dB scale. Therefore, imperfect CSI is expressed as $\hat{h} = h + \Delta h$ [23].

2.4 Theoretical Analysis for OFDM-IM under IQI

This section covers theoretical analysis for OFDM-IM in the presence of IQI at the receiver. Firstly, the impact of IQI on SINR for OFDM-IM systems is evaluated and compared with conventional OFDM. Later, ABEP is calculated for OFDM-IM considering IQI. In addition, computational complexity of the proposed technique is performed.

2.4.1 SINR Analysis

Regarding (2.13), desired signal $X(k)$ suffers from interference and amplified noise under IQI. Therefore, signal-to-interference ratio (SIR) regarding α and β parameters is expressed as

$$\gamma_I(k) = \frac{|\alpha|^2 E_s |H(k)|^2}{|\beta|^2 E_s |H^*(-k)|^2} = \frac{|\alpha|^2 \gamma_i(k)}{|\beta|^2 \gamma_i(-k)} \qquad (2.20)$$

where $\gamma_i(k) = \frac{E_s |H(k)|^2}{N_0}$ is the SNR per subcarrier for OFDM block, and E_s is the energy per symbol. The correlation between $\gamma_i(k)$ and $\gamma_i(-k)$ is assumed to be zero since the distance between k-th subcarrier and $-k$-th subcarrier is large [38]. So, SIR can be written as

$$\gamma_I = \frac{|\alpha|^2}{|\beta|^2}. \qquad (2.21)$$

Furthermore, the corresponding signal to interference noise ratio (SINR) is expressed as

$$\gamma(k) = \frac{|\alpha|^2 E_s |H(k)|^2}{|\beta|^2 E_s |H^*(-k)|^2 + (|\alpha|^2 + |\beta|^2) N_0}. \qquad (2.22)$$

Therefore, $\gamma(k)$ is expressed in terms of $\gamma_I(k)$ as follow

$$\gamma(k) = \frac{1}{\frac{|\beta|^2}{|\alpha|^2} + (1 + \frac{|\beta|^2}{|\alpha|^2})\gamma_i^{-1}} = \frac{1}{\gamma_I^{-1} + (1 + \gamma_I^{-1}) N_0}, \qquad (2.23)$$

where $\gamma_I^{-1} = \frac{|\beta|^2}{|\alpha|^2}$. γ equals to γ_i if $\beta = 0$ and $\alpha = 1$, which corresponds to zero IQI scenario. In contrast with OFDM, SIR for OFDM-IM γ_{I-IM} under IQI not only depends on IQI parameters but also subcarrier activation ratio $(\frac{a}{b})$. It is shown as

$$\gamma_{I-IM} = \frac{b}{a} \frac{|\alpha|^2}{|\beta|^2}, \qquad \gamma_{I-IM}^{-1} = \frac{a}{b} \frac{|\beta|^2}{|\alpha|^2}. \qquad (2.24)$$

Hence, OFDM-IM counters with less distortion caused by IQI, which is proportional to activation ration. In this sense, (2.23) converts to

$$\gamma_{IM} = \frac{1}{\gamma_{I-IM}^{-1} + (1 + \gamma_{I-IM}^{-1}) N_0}. \qquad (2.25)$$

2.4.2 ABEP Analysis

BER performance of OFDM-IM under IQI with maximum likelihood (ML) detector is evaluated by considering the pairwise error probability (PEP). The PEP results are valid for OFDM-IM with LLR receiver [7]. Only a single block is used to evaluate PEP, since all the subblocks are identical.

Conditional pairwise error probability (CPEP) of l-th subblock realization $\boldsymbol{X_l}$ being incorrectly detected as $\hat{\boldsymbol{X}}_l$ is given as [7]

$$P\left(\boldsymbol{X_l} \rightarrow \hat{\boldsymbol{X}}_l \mid \boldsymbol{H_l}\right) = Q\left(\sqrt{\frac{E_s \delta}{2N_0}}\right), \tag{2.26}$$

where $Q(.)$ is the Gaussian Q-function. $\boldsymbol{X_l}$ and $\boldsymbol{H_l}$ are $b \times b$ all zero matrix except for their diagonal elements which represent the data symbols and the CFR for l-th subblock, respectively. δ is represented as

$$\delta = ||(\boldsymbol{X_l} - \hat{\boldsymbol{X}}_l)\boldsymbol{H_l}||^2 = \boldsymbol{H_l^H A H_l}, \tag{2.27}$$

where $\boldsymbol{A} = (\boldsymbol{X_l} - \hat{\boldsymbol{X}}_l)^H(\boldsymbol{X_l} - \hat{\boldsymbol{X}}_l)$, and $(.)^H$ denotes the Toeplitz Hermitian matrix. In [7], an approximation of (2.26) is given as

$$P\left(\boldsymbol{X_l} \rightarrow \hat{\boldsymbol{X}}_l \mid \boldsymbol{H_l}\right) \cong \frac{e^{-\frac{E_s \delta}{4N_0}}}{12} + \frac{e^{-\frac{E_s \delta}{3N_0}}}{4}. \tag{2.28}$$

Therefore, the unconditional pairwise error probability (UPEP) is obtained by taking the expected value with respect to $\boldsymbol{H_l}$ as

$$P\left(\boldsymbol{X_l} \rightarrow \hat{\boldsymbol{X}}_l\right) \cong \boldsymbol{E_{H_l}}\left\{\frac{e^{-\frac{E_s \delta}{4N_0}}}{12} + \frac{e^{-\frac{E_s \delta}{3N_0}}}{4}\right\}. \tag{2.29}$$

The channel correlation in frequency domain is defined as follow $\boldsymbol{C} = \boldsymbol{E_{H_l}}\left\{\boldsymbol{H_l H_l^H}\right\}$, which equals $\boldsymbol{Q\Gamma Q^H}$ with $\boldsymbol{\Gamma} = \boldsymbol{E}\left\{\boldsymbol{cc^H}\right\}$ and $\boldsymbol{H_l} = \boldsymbol{Qc}$. Therefore, probability density function (PDF) of $\boldsymbol{c}$ is given as

$$f(\boldsymbol{c}) = \frac{\pi^{-r}}{det(\boldsymbol{\Gamma})} e^{-\boldsymbol{c}^H \boldsymbol{\Gamma}^{-1} \boldsymbol{c}}, \tag{2.30}$$

where $det(.)$ represents the determinant of a matrix, and r is the rank of $\boldsymbol{C}$. After combining (2.29) with (2.30), UPEP is given as [7]

$$P\left(\boldsymbol{X_l} \to \hat{\boldsymbol{X}}_{\boldsymbol{l}}\right) \cong \frac{1/12}{det(\boldsymbol{I} + \boldsymbol{C}\boldsymbol{A}\frac{E_s}{4N_0})} + \frac{1/4}{det(\boldsymbol{I} + \boldsymbol{C}\boldsymbol{A}\frac{E_s}{3N_0})}. \tag{2.31}$$

Regarding distortion and amplified noise in (2.25) due to IQI, the UPEP for OFDM-IM under IQI is expressed as

$$\begin{aligned} P\left(\boldsymbol{X_l} \to \hat{\boldsymbol{X}}_{\boldsymbol{l}}\right) &\cong \frac{1/12}{det(\boldsymbol{I} + \boldsymbol{C}\boldsymbol{A}\frac{E_s}{4(\gamma_{I-IM}^{-1} + (1+\gamma_{I-IM}^{-1})N_0)})} \\ &+ \frac{1/4}{det(\boldsymbol{I} + \boldsymbol{C}\boldsymbol{A}\frac{E_s}{3(\gamma_{I-IM}^{-1} + (1+\gamma_{I-IM}^{-1})N_0)})}. \end{aligned} \tag{2.32}$$

At last, the ABEP is calculated by considering all possible subblock realizations $\nu = 2^{p_1}$ of $\boldsymbol{X_l}$ and their pairwise error $\varepsilon(\boldsymbol{X_l}, \hat{\boldsymbol{X}}_{\boldsymbol{l}})$ as

$$P_e \cong \frac{1}{p\nu} \sum_{\boldsymbol{X_l}} \sum_{\hat{\boldsymbol{X}}_{\boldsymbol{l}}} P\left(\boldsymbol{X_l} \to \hat{\boldsymbol{X}}_{\boldsymbol{l}}\right) \varepsilon(\boldsymbol{X_l}, \hat{\boldsymbol{X}}_{\boldsymbol{l}}). \tag{2.33}$$

2.4.3   Complexity Analysis

From (18), complexity for α parameter estimation in terms of multiplications is

$$C_\alpha = N_B \cdot G \cdot min(a, b - a) \cdot 1C_{div}, \tag{2.34}$$

where C_{div} represents complex division, and it is assumed that one division equals to one multiplication. $min(a, b-a)$ denotes number of maximum used subcarriers in a subblock, which satisfy the condition ($X(k) \neq 0$ & $X(-k) = 0$ or $X(k) = 0$ & $X(-k) \neq 0$) to estimate the α and β parameters, respectively. As expressed in (19), estimation of β parameter requires the same complexity with α parameter,

and thus $C_\beta = C_\alpha$. According to (9), the computational complexity of the LLR detector is M multiplications per subcarrier [7]. Hence, the complexity of LLR receiver for N-size OFDM-IM block is NM multiplications. Total computational complexity of the proposed technique is

$$C_{total} = N_B \cdot (NMC_{mult} + 2 \cdot G \cdot min(a, b-a) \cdot 1C_{div}), \qquad (2.35)$$

where C_{mult} represents complex multiplication.

Figure 2.5: Comparison of theoretical SIR analysis and simulation results for OFDM-IM regarding to various subcarrier activation ratios and IQI parameters.

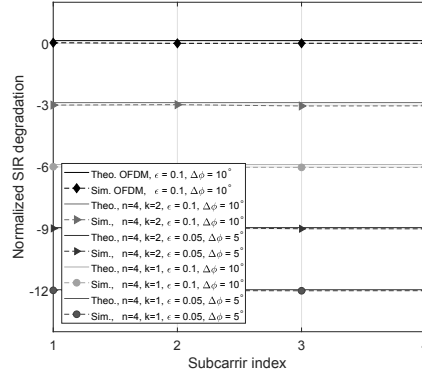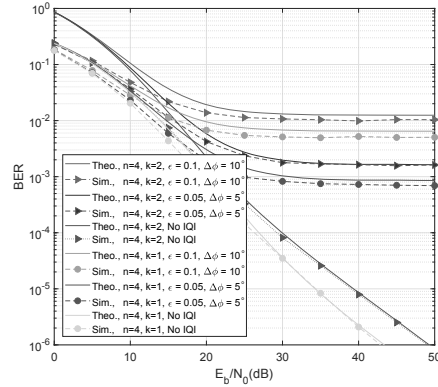

Figure 2.6: Comparison of theoretical BER analysis and simulation results for OFDM-IM regarding to various subcarrier activation ratios and IQI parameters.

2.5 Simulation Results and Analysis

In this section, performance of the proposed estimation and mitigation technique is evaluated for NB-IoT communication systems under IQI. Firstly, computer-based simulations are used to validate theoretical calculations for SIR and BER analysis. Later, performance of the proposed compensator is assessed by considering various subcarrier activation ratio in OFDM-IM and imperfect CSI. Moreover, computational complexity of the proposed non-iterative receiver is compared with state-of-the-art blind receivers [35]. The system parameters used in the simulations are $N = 256$, $L = 10$ and $CP = 16$. IQI parameters are adjusted as ($\epsilon = 0.05$, $\Delta\phi = 5°$) and ($\epsilon = 0.1$, $\Delta\phi = 10°$), which are faced in practical scenarios [43].

Obtained results of theoretical calculations for SIR degradation caused by IQI in OFDM-IM and OFDM are illustrated in Fig. 2.5. It is shown that SIR calculations perfectly match with the simulation results. OFDM-IM always is exposed to less distortion than classical OFDM thanks to partial subcarrier usage. Furthermore, OFDM-IM based systems offer the advantage to control the degradation of SIR due to IQI since it is proportional with subblock activation ratio (2.25). In Fig. 2.5, for IQI parameter ($\epsilon = 0.1, \Delta\phi = 10°$) a 3dB more degradation is observed between lines starting from orange line ($b = 4, a = 1$) to black line ($b = 4, a = 4$) since the activation ratio increases 2 times per line. Likewise, in Fig. 2.6 similar behavior is observed for theoretical BER results as calculated in (2.32) and (2.33). There is a difference between theoretical and simulation BER results for low SNR since the assumed approximations become inaccurate [7,31].

In order to show impact of different subcarrier activation ratios obviously, subblock size and number of active subcarriers are choosen as $b = 8$ and $a = 3, 5$, respectively. Spectral efficiency of OFDM-IM for ($b = 8, a = 3$) and ($b = 8, a = 5$) are the same with conventional OFDM, and equals to $\frac{m}{N+L} = 0.941$bits/s/Hz.

For all simulations in Fig. 2.7 and Fig. 2.8, active subcarriers carry BPSK modulated data symbols. "No IQI" refers to results without IQI, and "No Correction"

(a) IQI parameters ($\epsilon = 0.05, \Delta\phi = 5°$) (b) IQI parameters ($\epsilon = 0.1, \Delta\phi = 10°$)
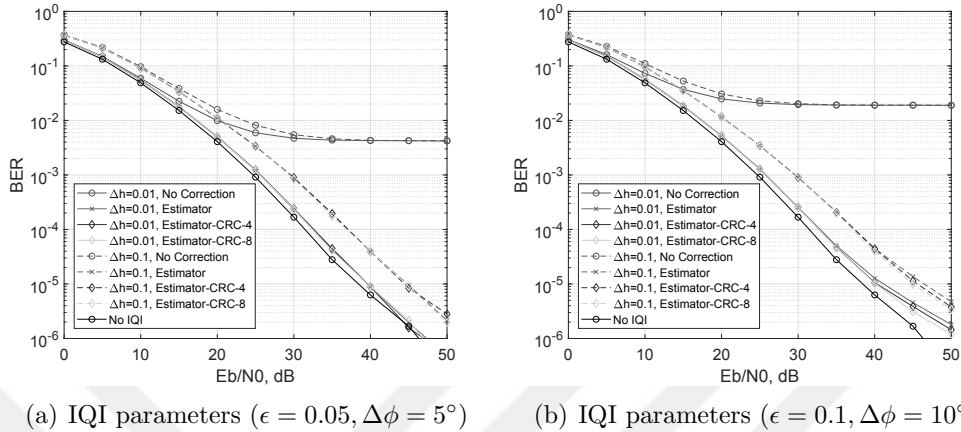
Figure 2.7: BER versus SNR performance for OFDM-IM with subblock parameters ($b = 8, a = 3$).

refers to results without the proposed compensator under IQI. "Estimator" refers to results with the compensator. In addition, estimator is combined with CRC algorithm to assess accuracy of decision on the selected subcarrier index status. "CRC-V" denotes V-number of CRC bits added to the end of OFDM-IM block. Moreover, two levels of imperfect CSI are used in the simulations as well as perfect CSI ($\Delta h = 0$). $\Delta h = 0.01$ refers to low error on CSI, while $\Delta h = 0.10$ represent high error on CSI. It is important to mention that in both Fig. 2.7 and Fig. 2.8, solid lines and dashed lines represent the results for $\Delta h = 0.01$ and $\Delta h = 0.1$, respectively.

In Fig. 2.7, OFDM-IM with ($b = 8, a = 3$) is simulated. Proposed non-iterative compensator by OFDM-IM perfectly mitigates low level IQI ($\epsilon = 0.05$, $\Delta\phi = 5°$), as shown in Fig. 2.7(a). Performance of the proposed compensator does not change with imperfect CSI, which causes shift for all the results regarding to level of imperfection (Δh). Subcarrier index status (active/inactive) is correctly detected since low activation ratio ($\frac{a}{b} = \frac{3}{8}$) leads to low SIR degradation caused by IQI. Hence, use of CRC bits does not further improve the BER performance for the proposed technique, as seen in the Fig. 2.7(a). Increase of the IQI parameters ($\epsilon = 0.1, \Delta\phi = 10°$) for the same activation ratio poses more degradation on BER performance, as illustrated in Fig. 2.7(b). The proposed compensator mitigates

19

(a) IQI parameters ($\epsilon = 0.05, \Delta\phi = 5°$) (b) IQI parameters ($\epsilon = 0.1, \Delta\phi = 10°$)
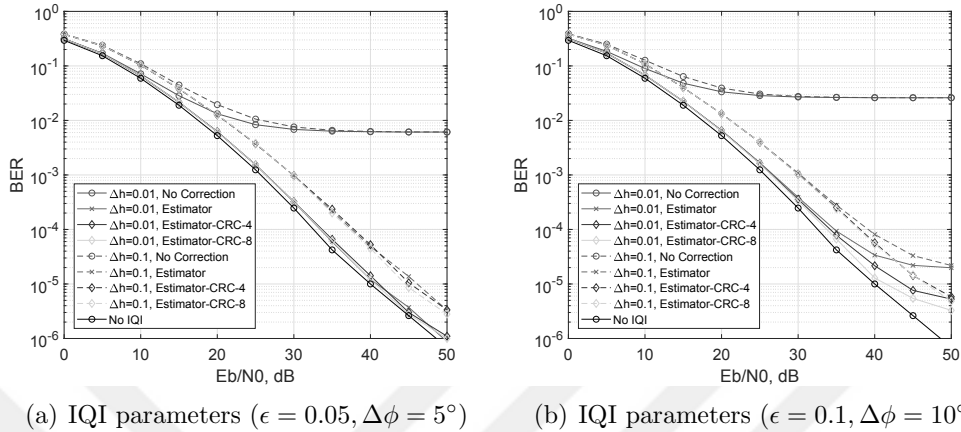
Figure 2.8: BER versus SNR performance for OFDM-IM with subblock parameters ($b = 8, a = 5$).

the impact of high IQI thanks to low activation ratio. Therefore, use of CRC algorithm is not required for low subcarrier activation ratios.

Although the same IQI parameters are used in Fig. 2.7 and Fig. 2.8, BER performance becomes worse in Fig. 2.8 due to increase on the number of active subcarriers ($b = 8, a = 5$). An activation ratio ($\frac{5}{8}$) increases the probability of facing both IBSD and IBII for a given subcarrier. Therefore, finding the right subcarrier index status becomes a challenge. In Fig. 2.8(a), the compensator provides similar results with Fig. 2.7(b) due to lower IQI parameters, even for higher activation ratio. In Fig. 2.8(b), the compensator has the worst performance since IQI level increases to ($\epsilon = 0.1$, $\Delta\phi = 10°$) as well as high activation ratio. Hence, reliability of estimated subcarrier index status decreases. Use of CRC bits to select utilized subcarriers increases the reliability, thus improvement is observed on BER. In addition, 8-bit CRC does not provide a considerable improvement on the BER with respect to 4-bit CRC. Hence, short CRC bit streams can be used for high subcarrier activation ratio and IQI level.

State-of-the-art blind estimators by utilizing least-mean-squares (LMS) and recursive-least-squares (RLS) are compared with the proposed technique, since the estimators are proposed for frequency independent IQI [35]. It is observed that two algorithms need around 1500 iterations to estimate IQI components.

Estimation by LMS and RLS algorithms need $5C_{mult}$ and $9C_{mult}$ per iteration, respectively. The computational complexity of the proposed method for the used system parameters ($a = 3, b = 8, \epsilon = 0.05$, $\Delta\phi = 5°$, $N_B = 1$) is $704C_{mult}$, according to (2.35). Estimation of IQI components is performed through one OFDM-IM block. However, averaging the estimation of IQI components over more than one block is needed for both high subcarrier activation ratio and IQI level ($a = 5, b = 8, \epsilon = 0.1$, $\Delta\phi = 10°$, $N_B = 5$). The results show that no more than 5 OFDM-IM blocks are required to estimate the IQI parameters, with computational complexity of $3520C_{mult}$.

In all figures, it is observed a significant degradation on the error performance when the IQI distorts the signal. The proposed non-iterative technique considerably mitigates the effect of IQI for OFDM-IM in NB-IoT communication systems.

2.6   Conclusion

NB-IoT devices require low hardware complexity, low cost and low power consumption for deployment flexibility. Use of DCR, which is recommended for NB-IoT, results in sensitivity against IQI. Hence, there is a need for solutions to mitigate IQI impact. In this paper, a practical receiver for IQI estimation and compensation is proposed, studied and evaluated both using computer simulations and theoretical analysis. Outcome of this work shows that proposed receiver mitigates IQI for NB-IoT. It is seen that almost perfectly mitigation for IQI faced in real scenarios. Therefore, we expect that our technique will be useful for NB-IoT applications. Unlike suppression techniques that are used in classical OFDM, where iterative approach is needed, a non-iterative approach is introduced. There is a critical difference between OFDM-IM and OFDM, which enables to use non-iterative approach on proposed receiver. In this specific study, we focus on NB-IoT, and therefore frequency independent IQI is studied. Further studies will investigate frequency-dependent IQI for wideband IoT systems.

Chapter 3

OFDM with Index Modulation for Asynchronous mMTC Networks

3.1 Introduction

Wireless communication systems can be classified into two fundamental categories, namely human-user-based and machine-user-based from the perspective of 5G use cases and applications [12, 51]. Current technology gives priority to human-based communications. However, the emerging idea of Massive Machine-Type Communications (mMTC) such as Internet of Things (IoT), vehicle-to-vehicle (V2V), vehicle-to-infrastructure (V2I), control of autonomous vehicles and smart cities with millions of sensors poses various demands for the next-generation networks [11, 16, 52]. mMTC, where a large number of machine users sporadically communicate with a given base station (BS), leads to asynchronous uplink transmission associated with multi-user interference (MUI). Hence, handling of asynchronous impairments is expected to be one of the most challenging problems for mMTC networks [11, 46, 51].

22

Orthogonal frequency division multiplexing (OFDM) has been well studied by academia in the last two decades [24]. It has been shown that OFDM is robust against inter-symbol interference (ISI) with the aid of cyclic prefix (CP), which turns the linear convolution with the channel into a circular convolution [34]. However, OFDM is severely effected from inter-carrier interference (ICI) due to loss of subcarrier orthogonality.

In multi-user OFDM, the users must be aligned in the time and frequency domains in order to maintain the orthogonality between the subcarriers. However, multi-user time alignment is infeasible in asynchronous mMTC-based systems, since signals transmitted from the users at different distances from the BS arrive with different time delays. Time misalignment causes ICI between the users. Furthermore, it is expected that the impact of MUI becomes significant when different power levels are assigned to the machine users, with respect to the applications or used cases [17]. Even if equal power is distributed to the users, as far as signals travel through different paths, power misalignment occurs at the BS.

In literature, 5G candidate waveforms including filter bank multi-carrier (FBMC), generalized frequency-division multiplexing (GFDM) and universal filtered multi-carrier (UFMC) are studied to relax MUI by suppressing out-of-band emission (OOBE) [19, 22, 45, 51]. Moreover, inserting guard-bands between the users is used to further suppress OOBE [17, 48]. However, filtering process increases the system complexity and use of guard-bands reduce spectral efficiency. In [42], a new perspective is presented to reduce MUI by clustering of the channel impulse response.

Recently, the proliferation of index modulation (IM) has introduced new research perspectives for 5G wireless systems [9]. At first, IM has been presented as spatial modulation technique (SM) for multiple-input multiple-output (MIMO) systems to convey information by antenna indices [33]. The notion of IM is also extended to OFDM and named as OFDM with index modulation (OFDM-IM), which carries information not only by data symbols but also by the indices of active subcarriers [3, 10]. In contrast to conventional OFDM, not all subcarriers are

utilized in OFDM-IM. In Figure 3.1, a simple example is illustrated for an OFDM-IM subblock consisting of eight subcarriers, where three of them are activated to convey data symbols. Extra bits are carried by the indices of active subcarriers to compensate inefficient use of spectrum. In addition, fractional subcarrier activation brings in diversity order as well as less energy consumption [9]. Hence, OFDM-IM provides a flexible and adaptive structure which can be optimized by considering the demands of next-generation communication systems.
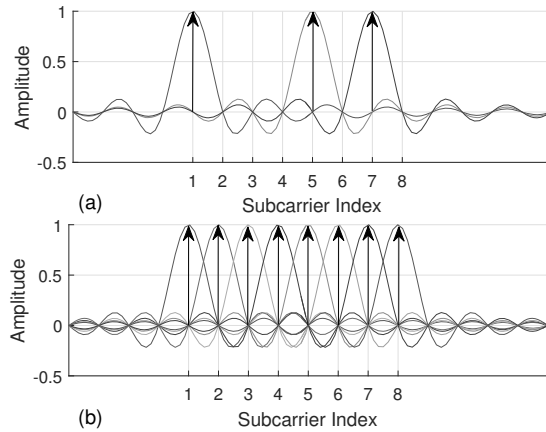
Figure 3.1: Frequency domain representation: (**a**) Three out of eight subcarriers are activated in OFDM-IM. (**b**) All of eight subcarriers are utilized in OFDM.

Mapping incoming bits to the subcarrier indices is one of the flexible properties of OFDM-IM. In the literature, three subcarrier mapping schemes (SMS) have been proposed to improve error performance and to reduce complexity of the OFDM-IM-based systems. Look-up table (LUT) is the first technique used as a mapping scheme, which uses same storage table at both transmitter and receiver [10]. However, it is not practical for large OFDM-IM subblock sizes. Therefore, Combinatorial method (COM), which does not require storage table, is proposed in [10]. Due to non-uniform subcarrier activation, COM leads to an unequal protection of the transmitted information bits that makes ultimate error performance worse. Hence, equiprobable subcarrier activation (ESA) technique is proposed in [50]. It is observed an enhancement up to 1.9 dB on error rate performance by using ESA for noisy multipath fading channels.

Performance of OFDM-IM is investigated under various impairments by researchers. In [10], it is shown that OFDM-IM under frequency selective fading channels impairment with high mobility is more robust than OFDM. Due to robustness against mobility, it is offered as a candidate for vehicle to X (V2X) communication systems [14]. ICI stemming from carrier frequency offset (CFO) impairment is evaluated by introducing notions of inter-subblock and intra-subblock interference for OFDM-IM [29]. It is observed that OFDM-IM is superior to current technology when the signal is impaired by CFO. In [37], both ICI and ISI is analyzed and mitigated using optimal tone spacing between adjacent subcarriers.

To the best of our knowledge, the performance of OFDM-IM under asynchronous transmission has not been characterized or investigated. In this paper, OFDM-IM is proposed as a candidate solution for uncoordinated mMTC networks. A novel subcarrier mapping scheme (ISA) is proposed to provide further enhancement of OFDM-IM performance for asynchronous systems. It is compared with the current ESA and COM mapping methods. The comparison is performed for various OFDM-IM subblock parameters to evaluate impact of flexibility properties of OFDM-IM. Not only time misalignment but also power difference between the machine users is considered in this study. In addition, ICI analysis is performed and the performance of the OFDM-IM is compared with conventional OFDM in the present of time and power offset between the users.

The remainder of this work is organized as follows. Section 3.2 introduces the multi-user OFDM-IM system model for asynchronous transmission. In Section 3.3, ICI analysis is provided for OFDM-IM. In Section 3.4, existing SMS are revisited and a novel mapping technique is proposed. Numerical results are given in Section 3.5. Finally, some concluding remarks are provided for OFDM-IM technology with mMTC in Section 3.6.

3.2 System Model

This section introduces an uplink system model where U users independently communicate with the base station (BS) through a frequency selective channel. A simple uplink system example is presented in Figure 3.2. Each user's information is modulated with OFDM-IM. A total of N subcarriers is equally split between the users, and $N_u = \frac{N}{U}$ subcarriers are dedicated to u-th user, with $1 \leq u \leq U$. Assignment of OFDM-IM subblocks to the users can be performed in two ways, either interleaved-based or localized-based. Interleaved-based assignment mixes the users' subblocks, while localized-based assignment successively places each user's subblocks, as visualized in Figure 3.2.
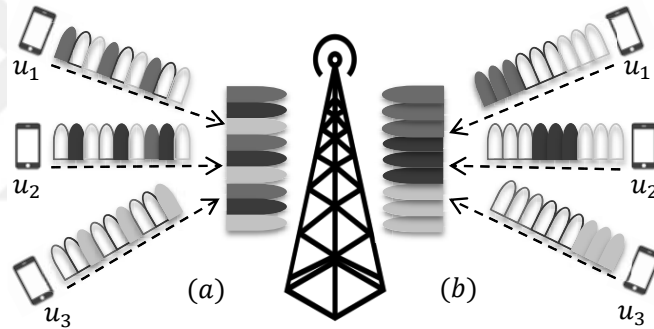
Figure 3.2: Uplink system model and user-subblock assignment methods; (**a**) interleaved; (**b**) localized. Each band represents an OFDM-IM subblock, which contains more than one subcarrier.

In Figure 3.3, time domain signal that belongs to u-th user is expressed as $x_u(n)$. It is assumed that $x_1(n)$, which reaches first to the BS, is considered to be reference signal for the BS. Each user's signal arrives to the BS with a different time offset (TO) ϵ_u with respect to $x_1(n)$ since they can be placed at different distances from the BS or can be transmitted at different times. The transmitted signal from each user passes through its own channel $h_u(n)$. All the channels are uncorrelated with each other. Later, individual signals $y_u(n)$ transmitted from all the users is superimposed, and additive white Gaussian noise (AWGN) $w(n)$ is

added to the superimposed signal $y(u)$. Due to the time misalignments, orthogonality between the machine users cannot be maintained anymore. Therefore, ICI between the users occurs and degrades the system performance. Further insights about asynchronous mMTC transmission with OFDM-IM are given in following subsection.
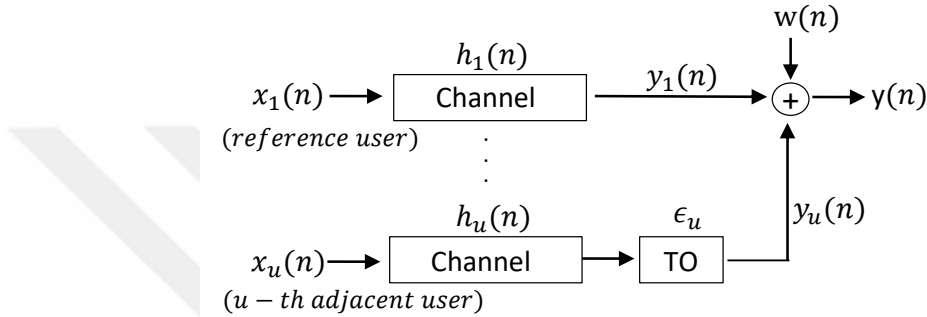
Figure 3.3: Baseband equivalent model of the uplink system by considering time offset between the users.

3.2.1 OFDM-IM Transmission Model

In this work, it is considered N size OFDM-IM block, where subcarriers are equally split into G subblocks. Each subblock consists of $s = \frac{N}{G}$ subcarriers and v out of s are selected to transmit M-ary data symbols with $1 \leq v < s$. As mentioned in Section 3.1, in contrast with conventional OFDM ($v = s$), not all subcarriers are utilized for M-ary symbols. Hence, the loss of spectral efficiency is compensated by the used subcarrier indices that convey additional information bits.

In multi-user transmission, each user has a total of $G_u = \frac{N_u}{s}$ available subblocks to carry m_u bit stream, with $1 \leq G_u \leq G$. When all the subcarriers are assigned to one user, G_u equals to G. Block diagram for asynchronous OFDM-IM transmitter is shown in Figure 3.4. Each OFDM-IM subblock consists of $p = \frac{m_u}{G_u}$ bit stream, which is divided into p_1 and p_2 bits. The indices of active subcarriers are defined from p_1 bit stream, while remaining p_2 bit stream is mapped

to conventional M-ary symbols $\{d_1, \ldots, d_v\} \in M_{ary}$, which are carried by the activated subcarriers. Division of the p bit stream is illustrated by "IM" entity in Figure 3.4. The indices of active subcarriers of u-th user for l-th subblock are defined as

$$\xi_u^l = \left[j_u(l, 1), j_u(l, 2), \ldots, j_u(l, v)\right]_{1 \times v} \tag{3.1}$$

where $j_u(l, v) \in [1, 2, \ldots, s]$ for $l = 1, \ldots, G_u$. Thus, total number of conveyed bits per OFDM-IM subblock is calculated as

$$p = p_1 + p_2 = \lfloor log_2(C(s, v)) \rfloor + v log_2(M) \tag{3.2}$$

where $\lfloor . \rfloor$ and $C(s, v)$ denote floor function and binomial coefficient, respectively. The number of transmitted bits per user is

$$m_u = G_u p = G_u \lfloor log_2(C(s, v)) \rfloor + G_u v log_2(M). \tag{3.3}$$

l-th subblock $c_u^i(l)$ belongs to i-th data block of u-th user is represented as

$$c_u^i(l) = \left[c_u^i(l, 1), c_u^i(l, 2) \ldots, c_u^i(l, s)\right]_{1 \times s} \tag{3.4}$$

where $c_u^i(l, s) \in \{0, M_{ary}\}$. M_{ary} represents the data symbols. Later, as illustrated by "Block Generator" in Figure 3.4, G_u subblocks are combined to form i-th data block of u-th user c_u^i expressed as follow

$$c_u^i = \left[c_u^i(1), \ldots, c_u^i(l), \ldots, c_u^i(G_u)\right]_{1 \times N_u}. \tag{3.5}$$

$V = vG_u$ out of $N_u = sG_u$ subcarriers carry M-ary symbols and the rest equal to zero. "IM" entity in Figure 3.4 full demonstrates the process of generating the frequency domain data samples for u-th user.
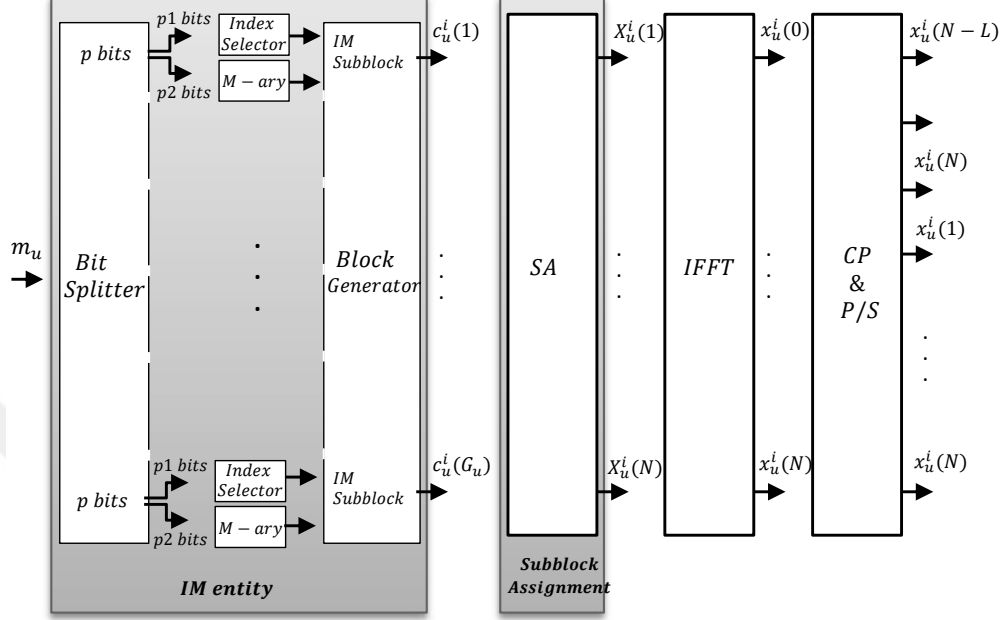
Figure 3.4: Block diagram of asynchronous OFDM-IM transmitter for i-th block of u-th user.

Once c_u^i is generated, it passes through the multi-user "Subblock assignment" (SA) entity, as in Figure 3.4. SA performs either localized assignment or interleaved assignment for c_u^i, and inserts N-N_u zeros to the subcarriers assigned to the other users. Then, i-th OFDM-IM block of u-th user is generated as follow

$$X_u^i = \left[0, \ldots, c_u^i(1), \ldots, 0, c_u^i(l), \ldots, 0, c_u^i(G_u), \ldots, 0\right]_{1 \times N}. \tag{3.6}$$

Time domain samples for i-th block of u-th user are obtained by inverse-Fast Fourier Transform (IFFT) process shown in Figure 3.4 as

$$x_u^i(n) = \sum_{k=0}^{N-1} X_u^i(k) e^{j2\pi nk/N}, 0 \leq n \leq N-1. \tag{3.7}$$

A cyclic prefix (CP) with length L is appended to the beginning of $x_u^i(n)$ to

prevent inter-symbol interference (ISI) due to time dispersion of the channel [34]. Time domain signal of u-th user $x_u(n)$ passes through multipath channel. The signal experiences Rayleigh fading. Channel impulse response coefficients between u-th user and the BS for i-th block are characterized as

$$h_u^i(n) = \sum_{r=0}^{L_{tap}-1} g_u^i(\tau_r)\delta(n - \tau_r) \tag{3.8}$$

where L_{tap} denotes total number of taps, r is the path index and τ_r is the delay of the r-th path. It is assumed that maximum excess delay of the channel is smaller than CP size, and path gains g_u^i are Gaussian random variables with distribution $\mathcal{CN}(0, 1/L_{tap})$. The signal $x_u(n)$ is received as

$$y_u(n) = x_u(n) * h_u(n) \tag{3.9}$$

where $*$ denotes convolution process. At the BS, signal transmitted from all the machine users are superimposed as follow

$$y(n) = \sum_{u=0}^{U-1} y_u(n - \epsilon_u) + w(n). \tag{3.10}$$

$w(n)$ is AWGN with distribution of $\mathcal{CN}(0, N_o/2)$.

At the receiver, time offset ϵ_u is removed from the superimposed signal to obtain the signal belonging to u-th user. Fast Fourier Transform (FFT) is applied to obtain the frequency domain samples $Y(k)$. Then, deassignment process, which refers to the inverse process of the SA, is applied to get only u-th user data blocks c_u. The indices of active subcarriers are detected by using maximum likelihood (ML) or log-likelihood ratio (LLR) detectors. ML detector checks all the possible subcarriers combinations and information symbols to find the most optimum joint decision. LLR receiver first detects active subcarriers and then information symbols carried by the detected subcarriers are demodulated [10].

3.3 ICI Analysis in OFDM-IM Systems

Consider a system model which includes $U = 3$ users with 3 OFDM-IM blocks to analyze ICI because of time offset ϵ between the users. These users transmit sporadically in adjacent bands with different transmit power levels, as illustrated in Figure 3.5a. For the sake of simplicity, it is assumed that equal time offset between the adjacent users. Notations of $b1$, $b2$ and $b3$ in the figure denote first, second and third OFDM-IM block, respectively.

In [46], ICI model is calculated for OFDM systems under time misalignment. Besides time offset, the model is modified for uncoordinated OFDM-IM systems by considering the fact that power difference between the machine users. In contrast to OFDM, only the active subcarriers of the users' cause ICI in OFDM-IM. Therefore, the indices of interferer subcarriers belong to ξ.
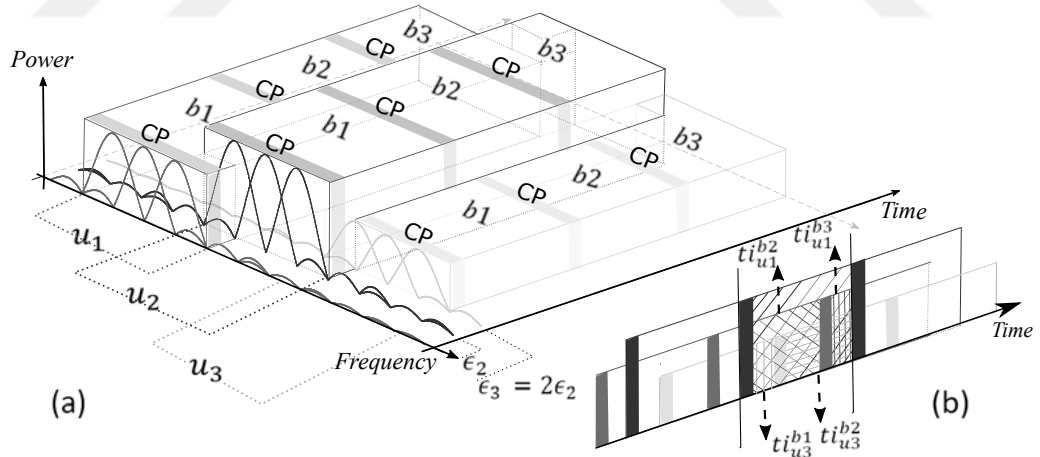
Figure 3.5: (**a**) Time, frequency and power domain illustration of three users' signals. (**b**) Time domain representation of the superimposed signal at the BS.

In our calculations, $ti_{u_y}^{u_x}$ shows the interference coming from u_x-th user to the u_y-th user while $ti_{u_x}^{bl}$ denotes the interference caused by l-th block of u_x-th user. ξ_u denotes the active subcarrier indices of u-th user for all the subblocks. Figure 3.5b shows the superimposed signal at the BS. As illustrated in the figure,

time domain interference for the 2-nd symbol of 2-nd user ti_{u_2} is calculated as

$$ti_{u_2} = ti_{u_2}^{u_1} + ti_{u_2}^{u_3}, \tag{3.11}$$

where $ti_{u_2}^{u_1} = ti_{u_1}^{b2} + ti_{u_1}^{b3}$ and $ti_{u_2}^{u_3} = ti_{u_3}^{b1} + ti_{u_3}^{b2}$, and they are expressed as

$$ti_{u_2}^{u_1}(n) = \sum_{n=0, n \in \xi_1}^{\epsilon-1} \sqrt{\Delta p_{12}}(-x_1^{b2}(n) + x_1^{b3}(n)), \tag{3.12}$$

$$ti_{u_2}^{u_3}(n) = \sum_{n=N-\epsilon+L, n \in \xi_3}^{N-1} \sqrt{\Delta p_{32}}(-x_3^{b2}(n) + x_3^{b1}(n)). \tag{3.13}$$

where Δp_{12} and Δp_{32} refers to power difference between the 1-st and 2-nd user, and the 3-rd and 2-nd user, respectively.

In the frequency domain, ICI I_2 is calculated by taking FFT for ti_{u_2}, and it is expressed as

$$I_2[k] = \sum_{k=0}^{N_u-1} ti_{u_2}^{u_1}(n)e^{-j2\pi kn/N} + \sum_{k=2N_u}^{3N_u-1} ti_{u_2}^{u_3}(n)e^{-j2\pi kn/N} \tag{3.14}$$

ICI for first user I_1 and third user I_3 is obtained as

$$I_1[k] = \sum_{k=N_u}^{2N_u-1} ti_{u_1}^{u_2}(n)e^{-j2\pi kn/N} + \sum_{k=2N_u}^{3N_u-1} ti_{u_1}^{u_3}(n)e^{-j2\pi kn/N}, \tag{3.15}$$

$$I_3[k] = \sum_{k=0}^{N_u-1} ti_{u_3}^{u_1}(n)e^{-j2\pi kn/N} + \sum_{k=N_u}^{2N_u-1} ti_{u_3}^{u_2}(n)e^{-j2\pi kn/N}. \tag{3.16}$$

As seen in the Figure 3.5b, by considering both time and power offset $ti_{u_1}^{u_2}, ti_{u_1}^{u_3}, ti_{u_3}^{u_1}$ and $ti_{u_3}^{u_2}$ can be easily extracted as

32

$$ti_{u_1}^{u_2}(n) = \sum_{n=N-\epsilon+L, n\in\xi_2}^{N-1} \sqrt{\Delta p_{21}}(-x_2^{b2}(n) + x_2^{b1}(n)) \qquad (3.17)$$

$$ti_{u_1}^{u_3}(n) = \sum_{n=N-2\epsilon+L, n\in\xi_3}^{N-1} \sqrt{\Delta p_{31}}(-x_3^{b2}(n) + x_3^{b1}(n)) \qquad (3.18)$$

$$ti_{u_3}^{u_1}(n) = \sum_{n=0, n\in\xi_1}^{2\epsilon-1} \sqrt{\Delta p_{13}}(-x_1^{b2}(n) + x_1^{b3}(n)) \qquad (3.19)$$

$$ti_{u_3}^{u_2}(n) = \sum_{n=0, n\in\xi_2}^{\epsilon-1} \sqrt{\Delta p_{23}}(-x_2^{b2}(n) + x_2^{b3}(n)) \qquad (3.20)$$

In this paper, it is considered that subcarriers belong to u-th user are orthogonal to each other while machine users' subcarriers are interfering with each other due to the time offset between them. For this reason, interference coming from other users to u-th user is mainly determined by its adjacent users' edge subcarriers. Since the subcarriers are sinc functions in frequency domain, inner subcarriers' sidelobes have less impact on the ICI compared to the edge subcarriers, as explained in [40, 41, 48]. Therefore, more users can be considered, but the interference coming from users that are not adjacent with the u-th user becomes much smaller.

3.4   OFDM-IM Subcarrier Mapping Schemes

In this section, the existing SMS-s in the literature for OFDM-IM are revised, and the proposed mapping scheme ISA is explained in details.

3.4.1 Existing SMS-s

3.4.1.1 LUT

The method requires at both transmitter and receiver side a look-up table with the size $d = 2^{p_1}$ to store all possible combinations of the active subcarrier indicies ξ with respect to p_1-bit stream. An example of LUT with $p_1 = 2$, $v = 2$ and $s = 4$ is illustrated in Table 3.1. $\beta(z)$ denotes bit streams corresponding to each index combination $\xi(z)$, with $z \in [1, 2 \ ... \ 2^{p_1}]$. The size of look-up table significantly increases the system complexity with the increase of the p_1. Therefore, LUT scheme become infeasible for large p_1.

Table 3.1: Look-up table for $(s = 4, v = 2)$.

β	ξ	I
00	1,2	$[X_l^1 \ X_l^2 \ 0 \ 0]$
01	2,3	$[0 \ X_2^1 \ X_l^3 \ 0]$
10	3,4	$[0 \ 0 \ X_l^3 \ X_l^4]$
11	1,4	$[X_l^1 \ 0 \ 0 \ X_l^4]$

At the receiver, ML detector is used to make a joint decision for active subcarrier indices with M-ary data symbols [10].

3.4.1.2 COM

In contrast to LUT method, storage tables at the transmitter and receiver are not required. It assigns a specific lexicographically ordered sequence $J(z) = \{\alpha_v, \ ..., \ \alpha_1\}$ with $\alpha \in \{0, \ ..., \ s - 1\}$ for each possible index combination $\xi(z)$. The $\beta(z)$-bit stream is converted to a natural number E, which is converted to a specific $J(z)$ sequence as follow

$$E = C(\alpha_v, v) \ + \ ... \ + C\ (\alpha_1, 1), \quad s > \alpha_v > ... \ \alpha_1 \geq 0. \quad (3.21)$$

To select α components, we start from the condition that satisfies $E \geq C(\alpha_v, v)$

and then choose the maximal α_{v-1} that satisfies $E - C(\alpha_v, v) \geq C(\alpha_{v-1}, v - 1)$ until $v = 1$ and then the index combination is obtained as $\xi(z) = J(z) + 1$. Detailed information about COM can be found in [10].

In the receiver, firstly $\xi(z)$ is identified for a given subblock by using LLR detector, and $J(z) = \xi(z) - 1$ is mapped to its corresponding decimal number E, which passes through bit to decimal converter to get $\beta(z)$ bit stream.

In Figure 3.6a,b subcarrier activation probability is represented by the red line for COM scheme. As seen in the figures, initial subcarriers have higher usage probability in comparison to the last ones, especially for $s = 8$ and $v = 3$.
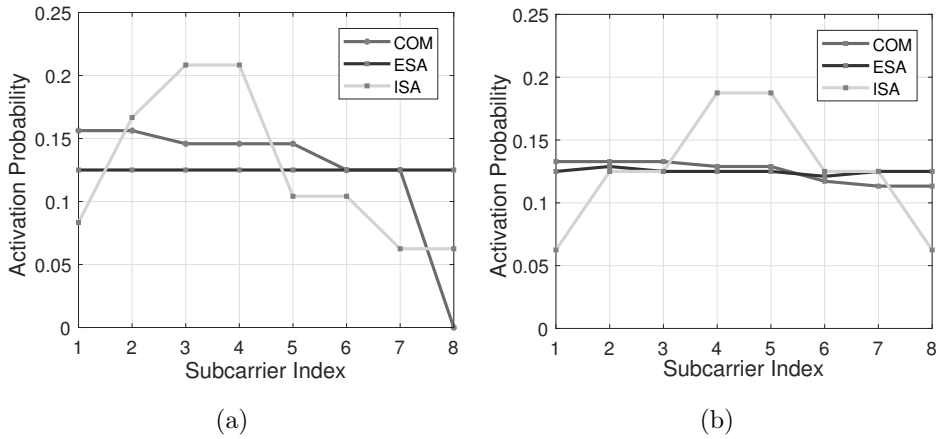
Figure 3.6: Subcarrier usage probability within an OFDM-IM subblock for the three SMS-s regarding to different (s, v). (**a**) $s = 8$ and $v = 3$. (**b**) $s = 8$ and $v = 4$.

3.4.1.3   ESA

In contrast with COM method, ESA offers as much as possible equiprobable subcarrier activation opportunity as illustrated in Figure 3.6a,b by the blue line [50]. A small table named as adjacent subcarrier distance vector (ASDV) is present at both transmitter and receiver to find $C(s - 1, v - 1)$ basic combinations ξ_b, which belongs to ξ. By using column cyclic shift $s - 1$ new active subcarrier combinations are generated from the ξ_b. The new combinations have the same ASDV with

the corresponding basic pattern ξ_b. Note that some index combinations generated from cyclic shift of ξ_b-s can be the same. In this case, ASDV considers only one from repeated patterns and disregards the rest. This idea successively is applied all over ξ_b until we get all 2^{p_1} possible subcarrier combinations ξ. Selection of the basic patterns ξ_b are explained in [50]. At the receiver side, LLR receiver is used to find $\xi(z)$ that is mapped to $\beta(z)$-bit stream for a given subblock.

3.4.2 Proposed SMS: ISA

Aforementioned SMS-s are designed for synchronous communication systems, which leads to equal noise power level at each subcarrier. Therefore, in this study new mapping scheme ISA, which stands for inner subcarrier activation, is proposed and explained to alleviate the ICI due to sporadic transmission in mMTC.

ISA scheme gives a higher activation probability to the subcarriers located at the center part of the OFDM-IM subblock, as illustrated in Figure 3.6a,b by the green line. OOBE coming from inner subcarrier is less than that of edge subcarriers [41]. Therefore, each user experiences less interference from its adjacent users.

ISA scheme is based on the COM scheme, which directly maps $\beta(z)$ bits to subcarrier indices $\xi(z)$, and vise versa. As calculated in line 1 of Algorithm 1, a subblock with s subcarriers is divided into two parts, where first part and second part contains s_1 subcarriers and s_2 subcarriers, respectively. v_1 subcarriers and v_2 subcarriers are activated to carry data information symbols. Indices for v_1 active subcarriers $\xi_1(z)$ are selected by flipped version of COM method, which is calculated from line 4 through 6. Conventional COM method is used to select v_2 subcarrier indices $\xi_2(z)$ as shown in line 7. Consequently, indices of active subcarriers for $\beta(z)$ are composed of $\xi_1(z)$ and $\xi_2(z)$, as shown in line 8. In ISA, p_1 equals $\lfloor log_2(C(s_1, v_1)) \rfloor + \lfloor log_2(C(s_2, v_2)) \rfloor \leq \lfloor log_2(C(s, v)) \rfloor$. This results in less spectral efficiency for some combinations of s and v.

At the receiver, LLR detectors are used to know the active subcarrier indices

Algorithm 1 ISA mapper.

1: $s_1 = \lfloor s/2 \rfloor$, $s_2 = s - s_1$ {# of subcarriers for each part}
2: $v_1 = \lfloor v/2 \rfloor$, $v_2 = v - v_1$ {# of active subcarriers for each part}
3: $\beta(z) = \begin{bmatrix} \beta_1(z) & \beta_2(z) \end{bmatrix}$ {Incoming bit stream}
4: $c = \begin{bmatrix} s_1 - 1 : -1 : 0 \end{bmatrix}$
5: $\xi_1(z) = COM(\beta_1(z), s_1, v_1)$
6: $\xi_1(z) = 1 + c(\xi_1(z))$ {Flipped version of COM}
7: $\xi_2(z) = v_1 + COM(\beta_2(z), s_2, v_2)$ { COM}
8: $\xi(z) = \begin{bmatrix} \xi_1(z) & \xi_2(z) \end{bmatrix}$ {Activated subcarrier indices}

$\xi(z)$, as shown in line 3 through 6 of Algorithm 2.

Algorithm 2 ISA demapper.

1: $s_1 = \lfloor s/2 \rfloor$, $s_2 = s - s_1$ {# of subcarriers for each part}
2: $v_1 = \lfloor v/2 \rfloor$, $v_2 = v - v_1$ {# of active subcarriers for each part}
3: $c' = \begin{bmatrix} 0 : 1 : s_1 - 1 \end{bmatrix}$
4: $\xi_1(z) = LLR(s_1, v_1)$
5: $\xi_1(z) = \xi_1(z) - 1, \xi_1(z) = sort(\xi_1(z),' ascend')$
6: $\xi_1(z) = c'(\xi_{11})$
7: $\xi_2(z) = LLR(s_2, v_2)$
8: $J_{z1} = \xi_1(z) - 1 \rightarrow E_1 \rightarrow \beta_1(z)$
9: $J_{z2} = \xi_2(z) - 1 \rightarrow E_2 \rightarrow \beta_2(z)$
10: $\beta(z) = \begin{bmatrix} \beta_1(z) & \beta_2(z) \end{bmatrix}$ {Bit stream}

The receiver first calculates the LLR values with respect to each subcarrier as

$$LLR(k) = log\frac{P(A_k)}{P(\overline{A_k})} + \frac{|Y(k)^2|}{N_0'} + log\frac{1}{M}\sum_{m=1}^{M}\frac{|Y(k) - H_u(k)d_m|}{N_0'}, \quad (3.22)$$

where $P(A_k)$ and $P(\overline{A_k})$ denotes the probability of k-th subcarrier being active and inactive, respectively. $N_0' = I_u + N_0$ shows total distortion of the system due to both ICI and noise, and $H_u(k)$ is channel frequency response (CFR) for u-th user. After calculation of LLR values for a subblock, v out of them with highest LLR define the active subcarriers. The subcarrier index patterns are converted to lexicographically ordered sequences J_{z1} and J_{z2}. By using Equation (3.21), these sequences are mapped to decimal numbers E_1 and E_2. Then, E_1 and E_2 undergo decimal-to-bit converter to obtain $\beta_1(z)$ and $\beta_2(z)$ bit streams as illustrated in line 7 and 8, respectively. $\beta(z)$ bit stream is a concatenation of $\beta_1(z)$ and $\beta_2(z)$, as shown in line 9.

Due to the fact that proposed ISA mapper is based on COM mapper, ISA does not bring additional complexity to the system. Unlike LUT and ESA schemes, storage tables are not required for ISA. Moreover, ISA technique gives higher activation probability $P(A_k)$ to the inner subcarriers with low N_0' and vice versa. Therefore, the reliability of calculated LLR values is maximum for asynchronous transmission with the aid of ISA regarding to Equation (3.22). In other words, detection performance of the active subcarriers under asynchronous transmission is increased by ISA.

3.5   Numerical Results and Discussion

This section is dedicated to evaluating the performance of OFDM-IM and OFDM-based systems for asynchronous mMTC networks. Theoretical results for ICI due to both time offset and power difference between the users are first validated by computer-based simulations. Secondly, BER performance for OFDM-IM with three different subcarrier mapping schemes including COM, ESA and ISA are shown to compare their performance for uncoordinated networks. In this study, we assume three users are sporadically transmitting to the BS. Available $N = 120$ subcarriers are equally split between the users. The system is tested over $L_{tap} = 10$ tap frequency-selective Rayleigh fading channel. A CP size is adjusted as $L = 30$ to prevent ISI for each user. BPSK modulation is used for the machine users. MATLAB software is used for the simulations.

In all simulations, two different subblock parameters are preferred to make a proper comparison between the subcarrier mapping methods. OFDM-IM with ESA for subblock parameters $s = 8$ and $v = 3$ offers the best performance in comparison to COM, since it benefits the most from frequency selectivity of the channel. On the other hand, the performance of ESA becomes similar to COM for the parameters $s = 8$ and $v = 4$ due to loss of selectivity, which is caused by usage of almost all subcarrier combinations [50]. In addition, two different time offset between the users are considered. Minimum and maximum time offset ϵ are adjusted as 24 and $(N + L)/2 = 75$, respectively. Power differences between

the users obey uniform distribution in a range of 2 dB and 7 dB.

In Figure 3.7, BER performance of existing SMS-s and the ISA are simulated for synchronous communication, where all users arrive to the BS at the same time ($\epsilon = 0$). Figure 3.7a shows the results for OFDM-IM with ($s = 8, v = 3$). ESA mapper is superior to COM mapper as aforementioned. BER performance of ISA lies in between COM with (s_1, v_1) and COM with (s, v) because of subblock division property. Therefore, the performance of ISA is the best for low signal-to-noise ratio (SNR). Its performance goes near to COM as SNR increases. In Figure 3.7b, obtained results are illustrated for ($s = 8, v = 4$). The performance of ESA is similar to COM [50].The performance of ISA is almost the same with ESA and COM for high SNR, while it outperforms for low SNR due to subblock division.
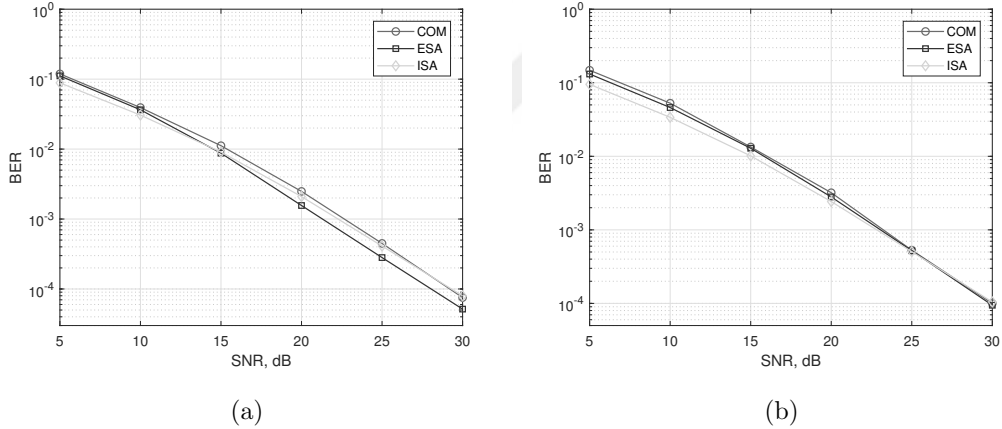

(a)   (b)

Figure 3.7: BER performance of synchronous multi-user OFDM-IM regarding to the three SMS-s. (**a**) SMS-s with $s = 8$ and $v = 3$. (**b**) SMS-s with $s = 8$ and $v = 4$.

In Figure 3.8, it is shown that theoretical calculations of ICI for both OFDM-IM and conventional OFDM perfectly match with computer-based simulations. The simulation results are obtained under maximum time offset $\epsilon = Max$ for 2-nd user, who has less power in comparison to others. As seen in the figure, OFDM-IM is exposed to less ICI thanks to partial subcarrier activation under asynchronous transmission. In the Figure 3.8a, the most exposed to ICI is ESA,

since it has higher probability of edge subcarrier usage as shown in Figure 3.6a. COM experience minimum ICI for initial subcarriers due to lower usage probability of last subcarriers of the previous user. On the other hand, last subcarriers of subblock are exposed to maximum ICI due to higher usage probability of initial subcarriers of the following user. Proposed method ISA encounters less ICI because of its lower usage probability for edge subcarriers. The obtained ICI results are inversely proportional to the edge subcarrier usage probability within the subblock. According to activation probability for SMS-s with ($s = 8$, $v = 4$) as in the Figure 3.6b, ISA faces minimum ICI, as illustrated in Figure 3.8b.
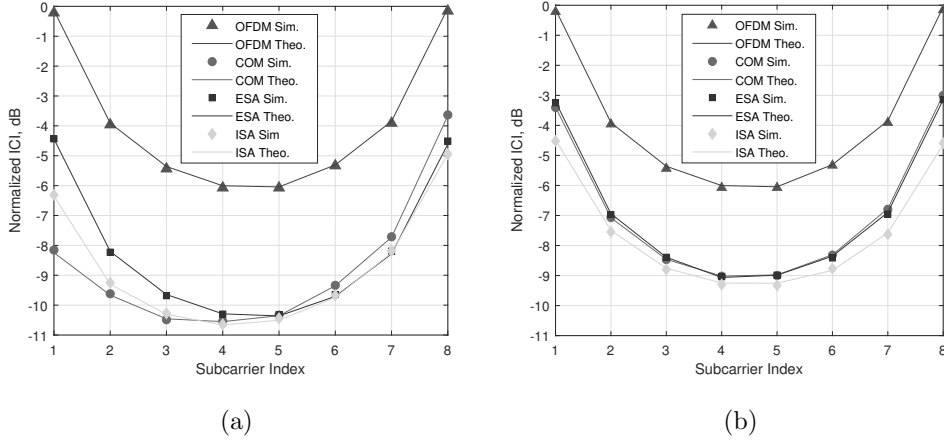
Figure 3.8: ICI analysis for OFDM and OFDM-IM regarding to three SMS-s. (**a**) SMS-s with $s = 8$ and $v = 3$. (**b**) SMS-s with $s = 8$ and $v = 4$.

In Figure 3.9, ICI analyzes on reference user are performed regarding different number of machine users with a fixed number of subcarriers per user. As seen in the Figure 3.9a,b, nearly 0.5 dB more interference is observed for 6 users compared with 3 users case. For more than 6 users, there is a very slit increase in the ICI. Hence, the amount of the interference coming from far users proportionally decays with the increase in the number of users.
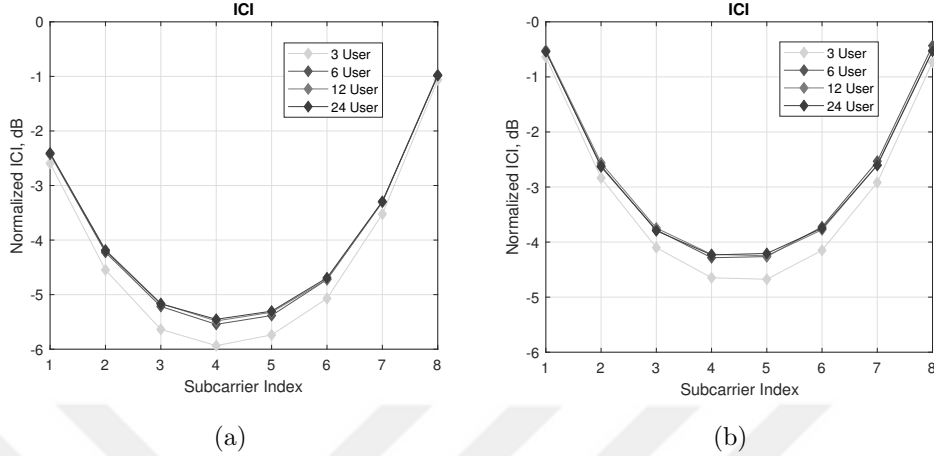
Figure 3.9: ICI analysis for ISA SMS regarding to various number of machine users. (**a**) ISA SMS with $s = 8$ and $v = 3$. (**b**) ISA SMS with $s = 8$ and $v = 4$.

In Figure 3.10, BER performances are obtained for 2-nd user under time and power misalignment. In Figure 3.10a,b, only time misalignment between the users is considered. As seen in the Figure 3.10a, ISA with ($s = 8$, $v = 3$) has the best BER performance, but with a slight difference from ESA for $\epsilon = Min$. Edge sub-carrier activation probability for ESA is higher in comparison to COM and ISA, as shown in Figure 3.6. Therefore, ICI coming from adjacent users to the 2-nd user further increases for ESA. For $\epsilon = Max$, the difference between the performances of SMS-s is more obvious and ESA has the worst performance. COM has a slight better BER performance than ESA as observed in the Figure 3.8b. ISA offers a much better BER performance for maximum time misalignment, since it has the smallest edge subcarrier activation probability associated with the lowest ICI. In Figure 3.10b, OFDM-IM with subblock parameters ($s = 8$, $v = 4$) is simulated. The performance of both ESA and COM become much worse than in Figure 3.10a. For ISA with ($s = 8$, $v = 4$), subcarrier usage probability is more localized around the middle subcarriers than in the case of ISA with ($s = 8$, $v = 3$), as shown in Figure 3.6. Moreover, equiprobable activation properties of ESA causes a destructive effect on the BER performance due to non-uniform distribution of ICI. For COM, less activation probability of one edge provides better protection against ICI caused by asynchronism between the users in time.

41

In Figure 3.10c,d, power difference between the users is also considered as well as time offset. The advantages of ISA against asynchronous transmission impairments are much more visible with the increase of ICI. Not only power difference but also increased number of active subcarriers within the OFDM-IM subblock results in higher ICI. Therefore, ISA mapping scheme plays a key role for larger subcarrier activation ratio of v/s in asynchronous mMTC networks.
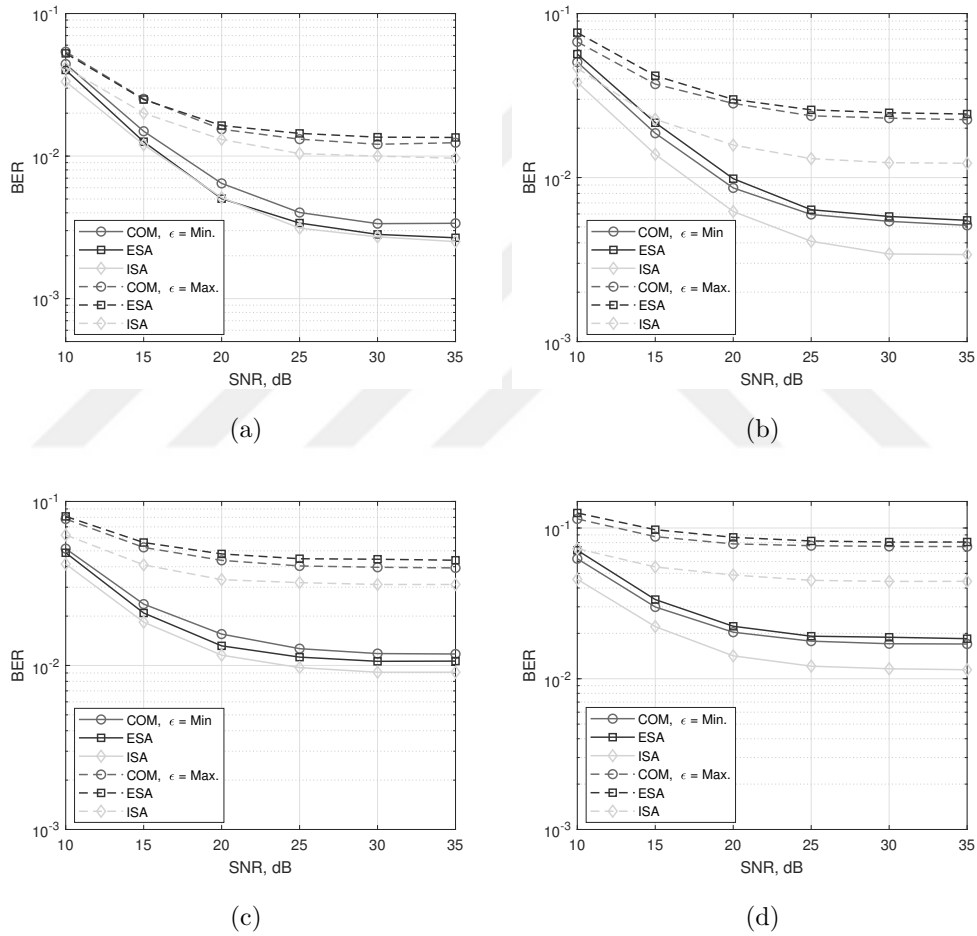

Figure 3.10: BER performance of multi-user OFDM-IM regarding to three SMS-s. Only time offset between the machine users is considered for (**a**) and (**b**), while both time and power offset are considered for (**c**) and (**d**). (**a**) SMS-s with $s = 8$ and $v = 3$. (**b**) SMS-s with $s = 8$ and $v = 4$. (**c**) SMS-s with $s = 8$ and $v = 3$. (**d**) SMS-s with $s = 8$ and $v = 4$.

3.6 Conclusions

One of the fundamental challenges for 5G and beyond technologies is to handle asynchronous impairments in uncoordinated mMTC networks. Performance of OFDM under time misalignment conditions is severely affected due to its susceptibility against ICI. Fractional subcarrier activation in OFDM-IM develops immunity to ICI caused by both time and power misalignments between the machine users. Flexible and adaptive structure of OFDM-IM provides opportunities to manage the active subcarriers. A novel subcarrier activation scheme ISA is proposed by considering the non-uniform distribution of ICI in asynchronous transmission. It offers the best performance in comparison to existing methods both COM and ESA without increasing the computational complexity. In addition, energy-free transmission through active subcarrier indices makes OFDM-IM technology a strong candidate for mMTC networks that require low energy consumption.

In this study, investigations are performed for OFDM-IM systems by considering asynchronous impact of mMTC networks. In order not to exceed the scope of this paper, OFDM-IM systems performance regarding other impacts of mMTC architecture is left for future studies. In the future work, we will consider both clustering users and conflicted users for mMTC. Moreover, optimization of OFDM-IM subblock size and activation ratio will be evaluated for different machine users with respect to their requirements.

Chapter 4

Conclusions

In this work, it is performed a detailed investigation of IQI with OFDM-IM for NB-IoT, and asynchronous transmission with OFDM-IM for mMTC. A list of specific contributions of this dissertation is given as follow.

1. IQI Mitigation for Narrowband IoT Systems with OFDM-IM

   - A practical receiver for IQI mitigation is proposed for NB-IoT with OFDM-IM based system.

   - OFDM-IM under IQI causes less SIR degradation in comparison with classical OFDM.

2. OFDM with Index Modulation for Asynchronous mMTC Networks

   - ISA mapping scheme is proposed to further alleviate ICI in asynchronous OFDM-IM-based systems.

   - OFDM-IM is proposed as an eligible solution to alleviate ICI caused by asynchronous transmission in uncoordinated mMTC networks.

Frequency-dependent IQI will be considered as a future research topic for wideband IoT.

Bibliography

[1] 3GPP TR 45.820 V13.1.0. Cellular System Support for Ultra Low Complexity and Low Throughput Internet of Things. Technical report, Nov. 2015.

[2] A.A. Abidi. Direct-conversion radio transceivers for digital communications. *IEEE J. Solid-State Circuits*, 30(12):1399–1410, Dec. 1995.

[3] Rami Abu-alhiga and Harald Haas. Subcarrier-index modulation OFDM. In *Proc. IEEE 20th International Symposium on Personal, Indoor and Mobile Radio Communications (PIMRC)*. IEEE, Sep. 2009.

[4] Ala Al-Fuqaha, Mohsen Guizani, Mehdi Mohammadi, Mohammed Aledhari, and Moussa Ayyash. Internet of Things: A Survey on Enabling Technologies, Protocols, and Applications. *IEEE Commun. Surveys Tut.*, 17(4):2347–2376, Apr. 2015.

[5] J. B. Andersen, T. S. Rappaport, and S. Yoshida. Propagation measurements and models for wireless communications channels. *IEEE Commun. Mag.*, 33(1):42–49, Jan. 1995.

[6] H. Arslan. IQ Gain Imbalance Measurement for OFDM Based Wireless Communication Systems. In *Proc. IEEE Military Commun. Conf. (MILCOM)*, pages 1–5, Oct. 2006.

[7] E. Başar, Ü. Aygölü, E. Panayırcı, and H. V. Poor. Orthogonal Frequency Division Multiplexing With Index Modulation. *IEEE Trans. Signal Process.*, 61(22):5536–5549, Nov. 2013.

[8] Ertuğrul Başar, Miaowen Wen, Raed Mesleh, Marco Di Renzo, Yue Xiao, and Harald Haas. Index Modulation Techniques for Next-Generation Wireless Networks. *IEEE Access*, 5:16693–16746, May. 2017.

[9] Ertugrul Basar. Index modulation techniques for 5G wireless networks. *IEEE Communications Magazine*, 54(7):168–175, Jul. 2016.

[10] Ertugrul Basar, Umit Aygolu, Erdal Panayirci, and H. Vincent Poor. Orthogonal Frequency Division Multiplexing with Index Modulation. *IEEE Transactions on Signal Processing*, 61(22):5536–5549, Nov. 2013.

[11] C. Bockelmann, N. Pratas, H. Nikopour, K. Au, T. Svensson, C. Stefanovic, P. Popovski, and A. Dekorsy. Massive machine-type communications in 5G: Physical and Mac-layer solutions. *IEEE Communications Magazine*, 54(9):59–65, Sep. 2016.

[12] Doug Brake. 5G and Next Generation Wireless: Implications for Policy and Competition. Technical report, Information Technology & Innovation Foundation (ITIF), Jun. 2016.

[13] A. Burdett. Ultra-Low-Power Wireless Systems: Energy-Efficient Radios for the Internet of Things. *IEEE Solid-State Circuits Mag.*, 7(2):18–28, Jun. 2015.

[14] X. Cheng, M. Wen, L. Yang, and Y. Li. Index modulated OFDM with interleaved grouping for V2X communications. In *Proc. 17th International IEEE Conference on Intelligent Transportation Systems (ITSC)*, pages 1097–1104, Oct. 2014.

[15] Xiang Cheng, Miaowen Wen, Liuqing Yang, and Yuke Li. Index modulated OFDM with interleaved grouping for V2X communications. In *Proc. IEEE 17th Int. Conf. Intell. Transp. Syst. (ITSC)*, pages 1–8, Oct. 2014.

[16] Nicola Cordeschi, Danilo Amendola, Mohammad Shojafar, and Enzo Baccarelli. Distributed and adaptive resource management in Cloud-assisted Cognitive Radio Vehicular Networks with hard reliability guarantees. *Vehicular Communications*, 2(1).

[17] A. F. Demir and H. Arslan. The Impact of Adaptive Guards for 5G and Beyond. In *Proc. IEEE International Symposium on Personal, Indoor, and Mobile Radio Communications (PIMRC)*, Oct. 2017.

[18] S. Doğan, A. Tusha, and H. Arslan. OFDM with Index Modulation for Asynchronous mMTC Networks. *Sensors*, 18(4):1–15, Apr. 2018.

[19] Mathieu Van Eeckhaute, André Bourdoux, Philippe De Doncker, and François Horlin. Performance of emerging multi-carrier waveforms for 5G asynchronous communications. *EURASIP Journal on Wireless Communications and Networking*, 2017(1), Feb. 2017.

[20] Ahmed ElSamadouny, Ahmad Gomaa, and Naofal Al-Dhahir. Likelihood-based spectrum sensing of OFDM signals in the presence of Tx/Rx I/Q imbalance. In *Proc. IEEE Global Commun. Conf. (GLOBECOM)*, pages 1–6, Dec. 2012.

[21] Ericsson. Cellular Networks for Massive IoT. Technical report, Jan. 2016.

[22] B. Farhang-Boroujeny. OFDM Versus Filter Bank Multicarrier. *IEEE Signal Processing Magazine*, 28(3):92–112, May. 2011.

[23] Jehad M. Hamamreh and Huseyin Arslan. Secure Orthogonal Transform Division Multiplexing (OTDM) Waveform for 5G and Beyond. *IEEE Commun. Lett.*, 21(5):1191–1194, May. 2017.

[24] T. Hwang, C. Yang, G. Wu, S. Li, and G. Y. Li. OFDM and Its Wireless Applications: A Survey. *IEEE Transactions on Vehicular Technology*, 58(4):1673–1694, May. 2009.

[25] Il-Gu Lee. Digital Pre-Distortion of Carrier Frequency Offset for Reliable Wi-Fi Enabled IoTs. *Future Internet*, 9(3):1–9, Mar. 2017.

[26] Yabo Li. *In-Phase and Quadrature Imbalance*. Springer New York, 2014.

[27] Chia-Ling Liu. Impacts of I/Q imbalance on QPSK-OFDM-QAM detection. *IEEE Trans. Consum. Electron.*, 44(3):984–989, Mar. 1998.

[28] Q. Ma, P. Yang, Y. Xiao, H. Bai, and S. Li. Error Probability Analysis of OFDM-IM With Carrier Frequency Offset. *IEEE Commun. Lett.*, 20(12):2434–2437, Dec. 2016.

[29] Qianli Ma, Ping Yang, Yue Xiao, Huirong Bai, and Shaoqian Li. Error Probability Analysis of OFDM-IM with Carrier Frequency Offset. *IEEE Communications Letters*, 20(12):2434–2437, Dec. 2016.

[30] H. A. Mahmoud, H. Arslan, M. K. Ozdemir, and F. E. Retnasothie. IQ Imbalance Correction for OFDMA Uplink Systems. In *Proc. IEEE Int. Conf. Commun. (ICC)*, pages 1–5, Jun. 2009.

[31] T. Mao, Z. Wang, Q. Wang, S. Chen, and L. Hanzo. Dual-Mode Index Modulation Aided OFDM. *IEEE Access*, 5(8):50–60, Aug. 2017.

[32] R. Y. Mesleh, H. Haas, S. Sinanovic, C. W. Ahn, and S. Yun. Spatial Modulation. *IEEE Trans. Veh. Technol.*, 57(4):2228–2241, Jul. 2008.

[33] R.Y. Mesleh, H. Haas, S. Sinanovic, Chang Wook Ahn, and Sangboh Yun. Spatial Modulation. *IEEE Transactions on Vehicular Technology*, 57(4):2228–2241, Jul. 2008.

[34] B. Muquet, Zhengdao Wang, G.B. Giannakis, M. de Courville, and P. Duhamel. Cyclic prefixing or zero padding for wireless multicarrier transmissions? *IEEE Transactions on Communications*, 50(12):2136–2148, Dec. 2002.

[35] W. Nam, H. Roh, J. Lee, and I. Kang. Blind Adaptive I/Q Imbalance Compensation Algorithms for Direct-Conversion Receivers. *IEEE Signal Process. Lett.*, 19(8):475–478, Aug. 2012.

[36] G. D. Ntouni, V. M. Kapinas, and G. K. Karagiannidis. On the Optimal Tone Spacing for Interference Mitigation in OFDM-IM Systems. *IEEE Commun. Lett.*, 21(5):1019–1022, May. 2017.

[37] Georgia D. Ntouni, Vasileios M. Kapinas, and George K. Karagiannidis. On the Optimal Tone Spacing for Interference Mitigation in OFDM-IM Systems. *IEEE Communications Letters*, 21(5):1019–1022, May. 2017.

[38] O. Ozdemir, R. Hamila, and N. Al-Dhahir. Exact Average OFDM Subcarrier SINR Analysis Under Joint Transmit-Receive I/Q Imbalance. *IEEE Trans. Veh. Technol.*, 63(8):4125–4130, Oct. 2014.

[39] Behzad Razavi. *RF Microelectronics.* Upper Saddle River, NJ, USA: Prentice-Hall, Inc., 1998.

[40] A. Sahin, E. Bala, I. Guvenc, R. Yang, and H. Arslan. Partially Overlapping Tones for Uncoordinated Networks. *IEEE Transactions on Communications*, 62(9):3363–3375, Sep. 2014.

[41] Alphan Sahin and Huseyin Arslan. Edge Windowing for OFDM Based Systems. *IEEE Communications Letters*, 15(11):1208–1211, Nov. 2011.

[42] Hossein Soleimani, Stefano Tomasin, Tohid Alizadeh, and Mohammad Shojafar. Cluster-head based feedback for simplified time reversal prefiltering in ultra-wideband systems. *Physical Communication*, 25(3):100 – 109, 2017.

[43] J. Tubbax, B. Come, L. Van der Perre, L. Deneire, S. Donnay, and M. Engels. Compensation of IQ imbalance in OFDM systems. In *Proc. IEEE Int. Conf. Commun., (ICC)*, pages 1–9, May. 2003.

[44] M. Valkama, M. Renfors, and V. Koivunen. Advanced methods for I/Q imbalance compensation in communication receivers. *IEEE Trans. Signal Process.*, 49(10):2335–2344, Oct. 2001.

[45] S. Wang, J. Armstrong, and J. S. Thompson. Waveform performance for asynchronous wireless 5G uplink communications. In *Proc 2016 IEEE 27th Annual International Symposium on Personal, Indoor, and Mobile Radio Communications (PIMRC)*, pages 1–6, Sep. 2016.

[46] S. Wang, J. S. Thompson, and P. M. Grant. Closed-Form Expressions for ICI/ISI in Filtered OFDM Systems for Asynchronous 5G Uplink. *IEEE Transactions on Communications*, 65(11):4886–4898, Nov. 2017.

[47] Y. P. E. Wang, X. Lin, A. Adhikary, A. Grovlen, Y. Sui, Y. Blankenship, J. Bergman, and H. S. Razaghi. A Primer on 3GPP Narrowband Internet of Things. *IEEE Commun. Mag.*, 55(3):117–123, Mar. 2017.

[48] T. Weiss, J. Hillenbrand, A. Krohn, and F.K. Jondral. Mutual interference in OFDM-based spectrum pooling systems. In *Proc. IEEE 59th Vehicular Technology Conference. VTC*, May. 2004.

[49] Miaowen Wen, Yuekai Zhang, Jun Li, Ertugrul Başar, and Fangjiong Chen. Equiprobable Subcarrier Activation Method for OFDM With Index Modulation. *IEEE Commun. Lett.*, 20(12):2386–2389, Dec. 2016.

[50] Miaowen Wen, Yuekai Zhang, Jun Li, Ertugrul Basar, and Fangjiong Chen. Equiprobable Subcarrier Activation Method for OFDM with Index Modulation. *IEEE Communications Letters*, 20(12):2386–2389, Dec. 2016.

[51] G. Wunder, P. Jung, M. Kasparick, T. Wild, F. Schaich, Y. Chen, S. T. Brink, I. Gaspar, N. Michailow, A. Festag, L. Mendes, N. Cassiau, D. Ktenas, M. Dryjanski, S. Pietrzyk, B. Eged, P. Vago, and F. Wiedmann. 5G NOW: Non-orthogonal, asynchronous waveforms for future mobile applications. *IEEE Communications Magazine*, 52(2):97–105, Feb. 2014.

[52] A. Yazar and H. Arslan. A flexibility metric and optimization methods for mixed numerologies in 5G and beyond. *accepted for publication in IEEE Access*, 2018.

OFDM WITH INDEX MODULATION FOR NARROWBAND IOT AND MMTC

ORIGINALITY REPORT

14%	**10**%	**10**%	**4**%
SIMILARITY INDEX	INTERNET SOURCES	PUBLICATIONS	STUDENT PAPERS

PRIMARY SOURCES

1	scholarcommons.usf.edu Internet Source	1%
2	Submitted to Nashville State Community College Student Paper	1%
3	www.arehna.di.uoa.gr Internet Source	<1%
4	repository.ntu.edu.sg Internet Source	<1%
5	Ertugrul Basar, Miaowen Wen, Raed Mesleh, Marco Di Renzo, Yue Xiao, Harald Haas. "Index Modulation Techniques for Next-Generation Wireless Networks", IEEE Access, 2017 Publication	<1%
6	tsukuba.repo.nii.ac.jp Internet Source	<1%
7	eprints.soton.ac.uk Internet Source	<1%